Yang Liu, An Deng, Mark Jaksa

Failure mechanisms of geocell walls and junctions

Geotextiles and Geomembranes, 2019; 47(2):104-120

Final publication at http://dx.doi.org/10.1016/j.geotexmem.2018.11.003

Failure Mechanisms of Geocell Walls and Junctions

Yang Liu [a], An Deng [a], Mark Jaksa [a]

[a] School of Civil, Environmental and Mining Engineering, the University of Adelaide, SA 5005, Australia.

[*] Corresponding author.

E-mail: yang.liu03@adelaide.edu.au

Phone: (+61 8) 8313 0591

Facsimile: (+61 8) 8313 4359

ABSTRACT

Geocell panels are honeycomb-like systems used to provide earth reinforcement. Strips of perforated high-density polyethylene sheets, also known as cell-walls, are welded together at locations known as junctions. The cell-wall and junctions are designed to support and transfer tensile and shear loads and the integrity of these is essential for the appropriate performance of geocells in practice. Nevertheless, there is no standardized test procedure to assess the strength of the cell-wall or junction, and limited research has been undertaken regarding the failure mechanisms of geocell panels when subjected to various loading scenarios. This paper aims to examine the responses of geocell junctions and cell-walls under various loading conditions. An extensive testing program was undertaken to assess the geocell junctions, which included uniaxial tensile, shear, peeling and splitting strength tests. The uniaxial tensile strength, trapezoidal tearing strength, and creep tests were carried out on the geocell walls. A ductility ratio was developed to measure the rapidness of failure

under different short-term loading scenarios for both the cell-wall and junction. This paper presents the observed failure patterns and an evaluation of the implications of the practical uses of geocells.

Keywords: Geosynthetics, geocell, cell-wall, junction, failure mechanisms

1. INTRODUCTION

Geocells have long proved effective in a wide range of geotechnical applications, such as earth retention, erosion control and roadways (Ngo et al., 2015; Song et al., 2017; Tanyu et al., 2013; Zhang et al., 2010). Most of today's commercial geocell products are comprised of three components: cell walls, junctions, and perforations (Figure 1). The cell walls are integrated by welding to form a honeycomb-like panel, to provide confinement for infill materials, such as sands and gravels. Geocells are supplied in a collapsed form and are outstretched on-site and anchored in place. The panel size and the cell space can be varied as part of the manufacturing process to suit individual requirements. The cell walls are commonly perforated to enhance drainage, to facilitate root growth between cells and to provide interlocking with coarse infills.

Geocells are typically subjected to gravity loads from the infill materials on steep slopes or channels (Wu and Austin, 1992). On a slope, as shown in Figure 2(a–c), both geocell junctions and cell-walls are subjected to soil action from all directions. In such scenarios, geocells can withstand high tearing, tensile and shear stresses in both the cell-wall and the welded junctions to prevent cell-wall rupture and separation of the junctions. In addition, similar loading conditions are common in other load-bearing structures such as pavement and railway track . Past studies (Dash and Shivadas, 2012; Hegde and Sitharam, 2015a; Hegde and Sitharam, 2015b; Liu et al., 2018; Shadmand et al., 2018; Suku et al., 2016; Tanyu et al., 2013; Venkateswarlu et al., 2018) have extensively evaluated the performance of geocell while very limited studies have reported on the response of geocell. Leshchinsky and Ling (2013) experimentally examined the performance of Novel Polymetric Alloy (NPA) geocell-reinforced ballast embankment under monotonic and cyclic loading conditions in which the geocell layer sustained cosmetic damage with slight bending at the top and bottom of the geocell; no tearing or rupture was found on the cell-wall and at the junction. Yang et al. (2012) observed junction failure when placing NPA geocell in the sand base layer of a pilot-scale unpaved road. Under cyclic traffic loading, the geocell layer experienced the loading scenario illustrated in Figure 2 (b) which resulted in splitting the welded junction. Similar failure mode was observed by Pokharel et al. (2010) who monotonically loaded a single unconfined NPA geocell.

The geocell junctions are critical features that support and transfer high loads. As a result, the junctions are situated in locations that are most vulnerable to damage and may result in unbalanced load transfer or even the failure of entire geocell panels (ASTM, 1993). Failure of the geocell junctions takes three forms: shear, where one strip is displaced longitudinally relative to the adjacent strip; peel, where one strip is displaced laterally; and tension, where two of the four strips at a junction are pulled relative to the other two and are perpendicular to the junction. However, there is a lack of standardized testing methods for geocells and a lack of detailed investigations into their failure mechanisms. According to the manufacturers' product specifications, the current testing method performed on geocells is limited to seam strength tests, as specified by ASTM (1993), which examines the weld strength by applying a uniaxial tensile force. A 200 mm long specimen, cut from a geocell panel, is secured in the jaws of a tensile testing apparatus and a tensile strain of 50 mm/min is applied continuously until the specimen fails. Consequently, design uncertainties and unforeseen failure patterns have impeded the application of geocell in some engineering fields, such as railway engineering. ASTM (1993) suggested that additional failure mechanisms could occur in cell-walls and junctions, and corresponding testing procedures are desired. However, these tests have not been implemented to date to assess the performance of contemporary geocell products.

There is also no established testing standard for assessing the integrity of cell-walls. Traditional testing methods for plastic materials may be adopted, but these are limited to short-term, uniaxial tensile strength tests. The potential failure mechanism that is likely to occur at the top or bottom edge of the geocell, as shown in Figure 2(a), has yet to be established. This type of failure occurs in the transition zone of embankment crests and slopes, where the geocell wall is subjected to a combination of flexure and tension. Where such damage occurs, the strength of the geocell wall is significantly compromised and subsequent soil movement can potentially result in global failure of the earth-reinforced embankment. Therefore, it is essential that the failure mechanisms of cell-walls, and their corresponding strength under tensile and flexural stresses, are investigated. In addition, permanent deformation has long been a concern in the use of geosynthetics in a variety of geotechnical applications (Becker and Nunes, 2015; Sawicki, 1998; Thakur et al., 2013). However, the long-term, creep behavior of geocell wall has yet to be assessed under tensile loading conditions.

This study incorporates a laboratory testing program to examine the failure mechanisms of geocell walls and junctions. In accordance with the likely failure modes discussed above, uniaxial tensile strength, trapezoidal tearing strength and creep tests were designed and conducted on cell-walls. Four tests, which reflect the loading conditions in practical use, were conducted on welded geocell junctions. The testing program included uniaxial tensile, shear, seam and peeling strength tests. To study the responses of geocells under various loading conditions, the stress-strain behaviors were measured along with the stiffness and peak and residual strengths. Different failure characteristics were observed from each test and were subsequently analyzed to derive the factors that affect geocell performance. Finally, this paper establishes and standardizes new testing procedures that will enable geocell manufacturers to measure and enhance the quality of existing geocell products, thereby increasing the reliability of geocell-reinforced systems.

2. EXPERIMENTAL PROGRAM

This section summarizes the tests involved in the program. Detailed specimen dimensions, testing procedures, and laboratory procedures are discussed.

2.1 Material

The experimental program was conducted on a perforated and textured commercial geocell product with a cell wall height of 100 mm. Each cell has a nominal opening area of 287 x 320 mm. The material specifications are obtained from the product brochure of a geocell manufacturer, the geocell section was fabricated using strips of high-density polyethylene (HDPE) sheet, with a density of 0.95 g/cm^3, determined in accordance with ASTM D1505 (ASTM, 2010). The geocell material incorporates carbon black for ultraviolet stabilization. The content by weight of carbon black is between 1.5% to 2%, which is homogeneously distributed throughout the material. The strips are textured (rhomboidal indentations), with a thickness of 1.52 mm (±0.15), in order to increase the friction at the interface with the infill material. The indentations are distributed at a surface density of 22−31 units per cm^2. The cell walls are perforated to enhance drainage and interlocking with the infill material. The cell-wall perforation proportion is 16.8% (±1%). Individual cells are connected using full-depth, ultrasonic spot-welds and aligned perpendicular to the longitudinal axis of the strip. Figure 3 presents the details of the geocell junction. The length of the weld melt-point is approximately 10 mm, with a spacing of 5 mm and an average width of 3 mm.

The typical stress-displacement relationship of HDPE, when loaded in uniaxial tension, is shown in Figure 4. It should be noted that this study adopts the conventional engineering stress calculation, which assumes that the stress and strain are distributed uniformly throughout the cross-section. There are two primary reasons for using this traditional approach. Firstly, most manufacturers use engineering stress to evaluate the strength and performance of their products. Secondly, it facilitates the comparison of the test measurements with the manufacturers' product specifications. As can be seen in Figure 4, the stress-displacement relationship typically exhibits three stages: A, B, and C. Stage A covers the elastic, post-yielding regions, and the peak tensile strength. It is followed by a post-peak softening stage (Zone B), where the specimen decreases in strength with only slight elongation. Subsequently, the load plateaus with continuous elongation, reflected by the specimen slightly gaining strength (Zone C).

2.2 Testing Procedures

Detailed testing procedures and configurations of each test are described in this section. It should be noted that all tests were performed using an Instron tensile machine at a temperature of 25º ± 5% and relative humidity of 50% ± 5%, to ensure that environmental effects were excluded.

2.2.1 Cell-wall: Tensile strength test

Uniaxial tensile strength tests were conducted on the plain area of the cell-wall in accordance with ASTM D638 (ASTM, 2004). The prepared specimens and testing details are shown in Figure 5. The gauge length of the specimens was 107 mm with a total of 58 mm gripping areas at both ends. The narrow section, where elongation occurs, was 13 mm in width. The purpose of conducting tensile strength tests on the cell-wall was to establish a reference against which the performance of the geocell junctions could be evaluated. The loading ranges of the Instron machine were set to 1,000 N in order to achieve optimal testing resolution. Once the specimen was clamped in place, the tensile force was applied by the displacement-controlled mechanism, at a rate of 50 mm/min. The elongation process continued until the specimen failed.

2.2.2 Cell-wall: Trapezoidal tearing strength test

Trapezoidal tearing strength tests were conducted on the cell-walls to evaluate the strength and failure mechanisms when edge damage occurs. The test was configured against ASTM (1996). Five identical specimens were prepared for this test; 75 mm high, 200 mm wide and 2 mm thick. Two white lines were marked on the specimen to indicate the locations of the edges of the custom-made clamps used to fix securely the specimen. The vertical spacing between the two lines was 50 mm on the left-hand side and 100 mm on the right-hand side. The cut was made at the center of the left-hand side of the specimen to mimic the damage induced by an in-operation tearing. The clamps were positioned diagonally so that the specimen could be torn apart from the left-hand side (i.e. the cut). The spacing between the two custom-made clamps was 300 mm prior to the start of the testing. As specified by ASTM (1996), in order to apply the tensile load, the Instron machine was set to displace at a fixed rate of 50 mm/min.

2.2.3 Cell-wall: Creep test

The design of the specimen was guided by ASTM (2016). The specimen sizes were slightly altered to suit the available geocell product and the bespoke loading apparatus. As shown in Figure 6, the specimen was 100 mm high and 200 mm wide, with a grip distance of 35 mm to ensure slipping did not occur during long-term loading. There were of a total 42, 10 mm diameter perforations in the specimen, accounting for 16.8% of the entire surface area of an individual cell-wall. These perforations reduce the strength of a cell-wall. Therefore, this particular location was chosen to be tested as it is the most vulnerable to external actions.

Figure 7 shows the rig used to perform the creep test. In order to maximize grip, the specimen was secured by a pair of clamps with screws penetrating the short edges. A linear variable differential transformer (LVDT) was installed on the face of the specimen to measure the strain rate of a fixed point, in the centerline of the specimen, and to obtain the specimen's elongation. The measurement is achieved by attaching a string to the lower clamp to transfer the differential movement between the upper and lower clamps to the LVDT and its associated recording device.

A total of five geocell specimens were tested for creep test, with different applied loads. The loads adopted were 60%, 65%, 70%, 80% and 90% of the ultimate tensile strength previously tested, which were calculated to be 0.49, 0.54, 0.58, 0.67, 0.75 kN, respectively. The specimens loaded at 0.67 kN (80%) and 0.75 kN (90%) loads ruptured at 50 mins and 30 mins, respectively, and therefore, these results are not presented in the study due to the short load application periods. The remaining specimens were loaded for up to 2 weeks (around 300 hours), as a consequence of other demands on the laboratory. After the 2-week loading phase, contraction in the longitudinal direction was also measured by the LVDTs, due to the high elasticity of the geocell material (HDPE). Although unloading is less likely to occur once a geocell is buried beneath the ground, the extent of contraction provides an insight into the post-loading behavior of geocells when cyclic loading is considered.

For each specimen, after approximately the 2-week loading period, the applied load was released from the specimen in a single operation. The LVDTs continued recording the displacements of three geocell specimens during and after unloading, to assess the shrinkage ratio. The shrinkage ratio is defined as the reduction in geocell height (mm) divided by the maximum elongation (mm) of each specimen (perpendicular to the height), at the cessation of the creep load application. Data acquisition was terminated once zero displacement was recorded by the LVDTs.

2.2.4 Junction: Tensile, shear, seam and split strength tests

Four types of test were conducted at the geocell junctions: direct tensile, shear, seam and split strength tests. The experimental configurations were designed in reference to ASTM (1993), with modifications to the specimen dimensions and setup. Since there is no standardized method available for these tests on geocell products, several specimens had to be prepared for each test for trial purposes. This enabled calibration of the dimensions of the specimens and the clamping system, to ensure that the forces were applied directly to the junction while providing sufficient interlock between the clamp and the geocell strips to prevent slippage and premature failure. At end of the trials, 40 mm was found to be the most secure length for gripping the specimens. The distances between the clamp tips were determined to be 10.5 mm for the tensile and shear strength tests, and 30 mm for the seam and split strength tests. These distances ensure that no pre-load was applied to the specimen prior to the commencement of actual testing. The specimens used in all tests were initially cut to the correct dimensions for the tensile and split strength tests. Then, the specimens for the shear strength and seam strength tests were trimmed to their final dimensions. The schematic drawings in Figure 8 show the loading scenario and the detailed configuration, including the clamping distance and clamp spacing. The corresponding laboratory setups are shown in Figure 9. These loading schemes mimic the three failure forms (shear, peel, and split) of the junctions, and examine their uniaxial tensile strength. The junction thicknesses of all specimens are summarized in Table 1. Each measurement was obtained at three locations along the specimen: top, bottom and middle, and average values were measured. Five replicates were initially prepared for each test. In case the results indicated clear discrepancies, additional specimens were tested, to facilitate a high level of consistency. The specimen designations for the junction and cell-wall tests are summarized in Table 2.

3. RESULTS AND DISCUSSION

This section summarizes the results of the testing program conducted on geocell walls and junctions. The results are presented in terms of engineering stress/axial force versus elongation, rather than stress-strain due to complexity resulting from different loading forms. Specifically, the stress-elongation relationship cannot be obtained for the cell-wall trapezoidal tearing strength test and the stress-strain relationship cannot be obtained for the junction split test. Implications of the results are discussed in relation to the practical implementations of geocells in geotechnical applications.

3.1 Cell-Wall: Uniaxial tensile strength

The plot of axial stress versus elongation of the cell-walls subjected to uniaxial tension is shown in Figure 10. The axial stress is calculated as the tensile load divided by the initial cross-sectional area of the specimen (19.5 mm^2). As can be seen in Figure 10, the initial ascending portion of all curves exhibited similar tendencies before reaching their corresponding peak tensile stresses at approximately 10 mm elongation. The tensile strengths of all specimens were very consistent; ranging from a minimum of 13.34 MPa to a maximum of 14.2 MPa. However, there were significant differences in the post-peak behavior among the five specimens tested, as a result of different failure modes. It can be seen that specimens 1, 2 and 4 did not exhibit the typical behavior of HDPE (Figure 4). These specimens failed relatively suddenly when compared to specimens 3 and 5.

Photographs taken during the tests were able to capture the different elongation modes, as shown in Figure 11. Although the loading rates of the specimens were identical (50 mm/min), specimens 1, 2 and 4 fractured at elongations approximately half of those exhibited by specimens 3 and 5. It can also be seen that the two subsets of specimens experienced different failure mechanisms. The failure of the specimen 3 in Figure 11(a) initiated from the right-hand-side edge, then propagated towards the center (as indicated by the red arrows) and the rupture point was at the left-hand-side edge. Whereas, specimen 5, in Figure 11(b), elongated vertically and exhibited significant elongation. In addition, the photographs of the failed specimens are shown in Figure 11(c) and (d). The post-failure forms of the 5 specimens exhibit good agreement with the corresponding stress-elongation relationship. For specimens 1, 2 and 4, the rupture surfaces (highlighted by red-dashed lines) are much sharper with little elongation, whereas specimens 3 and 5 failed more gradually.

It is worth mentioning that all specimens were treated with great care such that no damage was induced during the preparation stage. All specimens were extracted from the same location from different cell-walls and cut to the same sizes with the aid of a digital caliper (i.e. the thickness and width of each specimen were measured at three locations along the narrow section, and the variation in size was maintained within a tight tolerance of ±1%). Therefore, the different failure patterns can be attributed to the material itself, and most likely to the indented surface. Inconsistent distribution of ingredients throughout the material can result in variations in brittleness (e.g. less elongation indicates higher brittleness). As specified by the manufacturers, the tolerance of the depth of indentation is ±0.15 mm, which is ±9.8% of the designated thickness (1.52 mm). According to Meuller (2007), the surface structure of HDPE composite influence its post-yielding behavior; more rapid failure can occur at locations of stress concentration due to surface structural features, such as notches. For geocells, the deeper indentations acted as the equivalent of notches, which facilitated a brittle failure mode. This phenomenon is in agreement with previous studies (Choi et al., 2009; Meuller, 2007; Pan et al., 2017).

3.2 Cell-Wall: Trapezoidal tearing strength

According to ASTM (1996), the trapezoidal tearing strength is defined as the axial force versus the elongation of the cell-wall under tearing force. The test results are provided in Figure 12. In the pre-peak region, all specimens exhibited linear behavior. The recorded peak tearing strengths ranged from 5.02 MPa to 6.22 MPa. The post-peak behavior for all specimens exhibited similar and step-like functions. Post-peak, the axial force decreased due to the fracturing of the geocell section between two perforations. Subsequently, the applied tensile force was sustained by the adjacent geocell sections where the hardening was observed on the plot. This process repeated until the specimen fully ruptured. While no significant difference was observed in the tearing strength of the five specimens, there was a noticeable difference in the elongations, ranging from 157.2 mm to 222.9 mm. These differences can be partially attributed to the inconsistencies in the specimen, such as the spacing between perforations and the edge-to-perforation distances, as shown in Figure 13(a) and (b), respectively. It should be noted that cell-wall specimens A and B were randomly selected from a geocell panel and prepared to identical dimensions. In the photographs, the perforations shown are from the same cell-wall locations in specimens A and B and the distances/spacing were measured using a digital caliper and it is evident that slight, but nevertheless meaningful, variations exist between the two specimens. As the specimens fail in a progressive manner, the perforation spacing and edge-to-perforation distance have an important effect on the elongation (e.g. larger spacing resulted in higher elongations).

The cell-wall specimens failed in a progressive manner, where the material between two adjacent perforations ruptured sequentially, as shown in Figure 14(a-c). This failure pattern explains the stepped post-peak region of the force-elongation curves. Under the tearing force, all five specimens showed an identical failure pattern as shown in Figure 14(d). The solid arrow marks stage 1 of the failure, corresponding to stages of Figure 14(a) to (b) and the dashed arrow marks stage 2, corresponding to Figure 14(c). Both stages exhibited an inclined tearing pattern. Stage 1 initiated from the left-hand side (i.e. the cut) of the specimen, then the fracture path progressed in the upper-right direction. Once the elongation exceeded 120 mm, all specimens started fracturing from the right-hand side, initiating stage 2 fracturing. Overall, all specimens elongated more in stage 1 than in stage 2 of the failure process, resulting in the complete rupture at the upper-right-hand side. This can be attributed to the fact that the specimen had been elongated to an extent at which the tearing force had transitioned solely to tension.

3.3 Cell-wall: Creep test

The elongations and strains of three tested specimens are plotted against the elapsed time in Figure 15. The creep behavior of the three geocell specimens under different loads exhibits similar tendencies. This behavior can be divided into three stages: *A*, *B,* and *C*, in sequence. Stage *A* is defined here as *primary creep*, where the geocell specimens experienced a higher rate of elongation while a linear, axial strain versus time relationship was observed. For specimen 1 (0.49 kN loading) and specimen 2 (0.54 kN loading), the axial strain reached 7.5% and 6%, respectively, at the end of stage *A*, over a period of approximately 3 hours. Specimen 3 (0.58 kN loading) experienced a considerably higher axial strain (12.5%) during the initial 3 hours. Stage *B* is defined as *secondary creep*, where the rate of elongation decreased gradually for all three specimens; hence, the strain-time relationships formed smooth curves. The durations of stage *B* for specimens 1 and 2 were similar. Both specimens entered their final stages after approximately 55 hours, while their axial strains reached 15%. Specimen 3 experienced significantly higher elongation during stage *B*, reaching approximately 28% axial strain. Stage *C* is defined as the period when all specimens returned to an approximately linear trend with minimal fluctuations. It can be seen that specimen 3 exhibited a higher elongation rate than specimens 1 and 2. The axial strains of all three specimens peaked at 17.7% (24.8 mm), 19.5% (27.4 mm) and 63.2% (65.2 mm), respectively, at approximately 300 hours prior to unloading. With all things considered, in comparison to specimen 1, the additional 0.05 kN applied to specimen 2, was unable to cause a significant increase in elongation, which was merely 2.5 mm longer. However, specimen 3 exhibited a dramatically higher elongation when compared to both specimens 1 and 2, which were 40.3 mm and 37.9 mm longer, respectively.

All specimens became stable within approximately 1.5 hours of unloading and were then removed from the test apparatus. The specimen shrinkage was recorded by the LVDT and this is reflected in Figure 15 (a). The final forms of the three specimens are shown in Figure 16. Based on visual observations, specimen 1 [Figure 16(a)] returned almost entirely to its pre-loading form. A slight elongation can be seen in the perforations, but no deformation was evident from the creep loading. Specimen 2 [Figure 16(b)] deformed and deflected slightly along its edge, particularly in the area adjacent to the perforations. However, its structure and geometry remained sound, as no damage was observed. Specimen 3 exhibited minor ruptures adjacent to the edge-perforations, as outlined in yellow in Figure 16(c). The specimen was significantly twisted and stretched, and failure was expected to occur if the loading period or weight was increased. Table 3 summarizes the shrinkage ratios of the three tested specimens. The shrinkage ratio is inversely proportional to the loading value. Specimen 3 exhibited the lowest shrinkage ratio, 53.0%, while specimens 1 and 2 contracted by 79.3% and 61.5% respectively.

3.4 Junctions: Tensile strength

The plot of axial stress versus elongation of both the geocell wall and junctions, subjected to uniaxial tension, is shown in Figure 17. Firstly, there is a noticeable difference in behavior between the junction specimens and the cell-wall strips, which is reflected by a more rapid increase in the elastic region and a sharper strength reduction in the plastic region. Among the five junction specimens, specimens 2 to 4 exhibited a similar tendency in the post-peak region, with an insignificant difference in the rate of strength reduction and elongation at failure, while only specimen 1 experienced much less ductile behavior, resulting in only 23.5 mm elongation prior to failure.

Additionally, a higher tensile strength was expected for geocell junctions, considering the fact that the geocell junction is the welded formation of two cell-wall strips. Nevertheless, there was no significant increase in the tensile strength observed at the geocell junctions. The tensile strengths of the junction specimens ranged from 15.9 MPa to 16.5 MPa, while the cell-wall strips varied between 13.34 MPa and 14.2 MPa, which equates to a modest increase of less than 20%. This can be attributed to the welded joint generally having a lower tensile strength when compared to the HDPE material itself (Tariq et al., 2011); hence it cannot provide a significant improvement in the tensile strength of a geocell junction.

Two failure modes were identified for geocell junctions under tensile loading, which can be observed in Figure 18(b) and (c). All specimens experienced identical behavior in their initial stage of failure, with the elongation initiating from approximately the middle of the welds, as shown in Figure 18(a). The initial stage was then followed by two different failure modes. Specimens 2-4 continued elongating in a vertical manner until rupture occurred. Whereas, for specimen 1, the fracture was initiated from the left-hand-side after reaching its peak tensile strength and followed by rupture which propagated towards the right-hand edge. Similar failure modes were observed on the cell-wall which was attributed to the stress concentration caused by inconsistent indentation depths (cf §3.1 Cell-Wall: Uniaxial tensile strength). These observations agree with the discrepancy in Figure 17 and provide an explanation for the brittle failure mode of specimen 1.

3.5 Junction: Shear strength

The plot of shear stress versus elongation of the geocell junctions subjected to a shear force is shown in Figure 19 (black lines). It can be seen, of the five specimens tested, most exhibited similar behavior. The shear stress increases almost linearly before peaking, and this is followed by a relatively sudden failure, reflected by less elongation when compared with the other tests conducted on the junction. There are only small differences between the measured peak shear strengths; ranging from 2.58 MPa to 2.98 MPa. However, some discrepancy is found in the post-peak region, reflected by different rates of strength reduction. The elongations at rupture ranged from 18.3 mm to 31.4 mm.

All specimens experienced similar failure modes, where the rupture occurred adjacent to the junction, as shown in Figure 20. This indicates that the junction is unlikely to fail during shearing and the shear strength of the junction is significantly higher than the peak shear stresses obtained from the present experimental program, yet it is more vulnerable to tensile stress. This observation is confirmed by the elongation mode in Figure 20(b), where the specimen deformed only in the cell-wall strip, while the junction remained intact. Therefore, it is worthwhile to investigate the tensile strength of the cell-wall strips induced by the shearing action, and the tensile stress versus elongation relationships are plotted in red in Figure 19. Interestingly, under the action of shear, the tensile strength of the cell-wall was considerably higher than the tensile strength of a simple cell-wall specimen (cf §3.1 Cell-Wall: Uniaxial tensile strength). The former had a tensile strength ranging from 18.1 MPa to 21.7 MPa, while the latter had a tensile strength ranging from 13.3 MPa to 14.2 MPa, equating to an average increase of 42%. The welded junction provides additional resistance to the cell-wall against tension, which assists the cell-wall area near the junction to support, for example, gravity loads caused by soil movement (Figure 2).

3.6 Junction: Seam Strength

The plot of stress versus displacement of the geocell junctions, when subjected to a peeling force, is shown in Figure 21. All five tested specimens exhibit a similar trend, with a reduced rate of increase in the elastic region, followed by a dramatic strength reduction. The maximum recorded seam strength is 8.21 MPa while the minimum seam strength 7.5 MPa across five specimens, resulting in a less 10% variation. Under the action of peeling, two failure modes were observed, as are shown in Figure 22. Only one (specimen 1) of the five tested specimens experienced weld fracture [Figure 22(c)], while the other specimens failed in the cell-wall adjacent to the weld junction. This specimen 1 (J-SMS-1) also experienced the most fluctuations throughout the loading process, as can be seen in Figure 21. Due to the low possibility of occurrence of this failure mode, it is considered that this is likely the result of faulty/unsatisfactory welding during manufacturing.

3.7 Junction: Split strength

The split strength test is of particular interest to this study. Unlike other loads, which occur less frequently when the geocell is placed in the field, such as in the case of pavement or slopes, the junctions are constantly subjected to a splitting force. The axial stress versus elongation results are shown in Figure 23. The tensile stress is calculated as the tensile force divided by the initial longitudinal cross-sectional area (262.5 mm^2) of the geocell junctions. All of the results exhibit a similar nature, with variations in peak stresses and post-peak behavior. Interestingly, although the loading mechanism of the splitting force is similar to that of the peeling force, the geocell behaved differently, with significant differences in peak strengths. The minimum splitting strength (3.69 MPa) varied slightly from the maximum value (4.03 MPa). Almost all specimens experienced a rapid stress reduction post-peak, while specimen 4 increased in stress for a short period, followed by a rapid failure.

Two types of failure mechanisms were observed, as shown in Figure 24. The failure mode that is shown in Figure 24(b) can be described as occurring when the two welded, cell-wall strips completely separated from each other due to rupture of the weld. The failure mode that is shown in Figure 24(c) is defined as cell-wall failure, as the junction did not fail under the influence of the splitting force. The latter mode is similar to the failure condition under shearing and peeling. It should be noted that geocell junctions exhibit a higher splitting strength when the junctions experience the failure mode of complete separation. This mode was exhibited by specimens 1 and 5, which recorded the highest splitting strengths of 3.98 MPa and 4.03 MPa, respectively.

As the stress-displacement relationship was obtained from the seam strength tests, the geocell junctions reached their peak strength under the splitting load, significantly slower than in other loading scenarios. This phenomenon suggests that, when geocells are used in the field (such as in slope protection), it is possible that the soil structure will experience a gradual down-slope movement prior to failure if the gravitational load exceeds that specified by the manufacturer. The post-peak behavior suggests that, once the junction reaches its splitting strength, failure occurs faster when compared with other loading conditions.

3.8 Ductility ratio

To assess the rate of failure in both cell-walls and junctions under short-term loading scenarios, a ductility ratio is proposed. This relationship entirely focuses on elongation and is not relevant to strength. First, the ductilities of the elastic and plastic regions are obtained from the elongations in two respective regions over the original gauge length. The ductility ratio is then calculated as the ductility of the plastic region divided by the ductility of the elastic region. Higher values indicate that the specimen reaches its peak strength quicker and experiences a less dramatic strength reduction. Figure 25(b) summarizes the strength versus pre-peak elongation relationship for all tests conducted on the cell-walls and junctions. The plot is helpful in evaluating the elastic response of geocells under different loading scenarios. As can be seen, the junctions provided similar strength against shear, peeling and splitting whilst also summarizes the ductility ratios of all test schemes examined in the present study. An average ratio is adopted for each test scheme.

As can be seen in Table 4, the splitting and seam strength tests are both associated with extremely low values, which signify that the geocell junctions are more prone to failure when subjected to peeling and splitting forces (as demonstrated in this study; cf §3.6 and §3.7). These two loading scenarios may be the most typical in practical applications of geocells. The trapezoidal tearing strength tests yielded a better ratio of 2.61, which also suggests that the geocell wall is vulnerable to tearing forces even when the cell-wall is slightly damaged. The geocell junctions showed superior performance under tension and shearing, returning ductility ratios of 12.17 and 12.18, respectively. Plotting the pre-peak elongation against the post-peak elongation [(Figure 25(a)] provides a more direct interpretation of the ductility ratio, reflected by the locations of these data points. Being closer to the origin suggests lower resilience relative to its corresponding loading type due to small overall elongation.

Figure 25(b) summarizes the strength versus pre-peak elongation relationship for all tests conducted on the cell-walls and junctions. The plot is helpful in evaluating the elastic response of geocells under different loading scenarios. As can be seen, the junctions provided similar strength against shear, peeling and splitting whilst also exhibiting the highest ductility with respect to shear and the highest strength associated with uniaxial tension. This implies that geocell is most vulnerable against shear. In addition, the cell-wall performed well when subjected both to uniaxial tension and tearing, reflected by reasonably long elongation prior to achieving its peak strength.

4. CONCLUSIONS

This study assesses the failure mechanisms of geocells when subjected to tensile and shear loads. An experimental program, which involved six test schemes, were conducted on the cell-walls and welded junctions of the geocell.

The experiments involved the application of uniaxial tension to cell-wall strips to assess their tensile capacity and creep behavior, while the junctions were subjected to four loading types: uniaxial tension; shear; peeling; and splitting. The stresses and elongation of the samples were recorded to evaluate the peak strength, and the behaviors of both the cell-wall and junctions in the elastic and plastic regions. The failure modes for all loading scenarios were observed, and the implications for the operational deployment of geocells were discussed.

This study draws the following conclusions:

1. Cell-walls behave inconsistently under uniaxial tension, mainly in the post-peak region. This is reflected by some specimens exhibiting a considerably rapid strength reduction in the post-peak region, while the others exhibited behavior typical of the HDPE material. This is a result of stress concentrations caused by inconsistent indentation depth in the cell-wall.
2. Although the junctions of geocells are formed by welding two cell-wall strips, there was no significant, observed increase in tensile strength. All specimens failed relatively quickly after reaching their tensile strength.
3. The trapezoidal tearing strength was assessed using pre-cut, cell-wall specimens. All specimens failed in a progressive and diagonal manner, following the pattern of the perforations. The pre-cut specimens performed better than expected, reaching their peak tearing strength at approximately 50 mm of elongation before the first rupture occurred. The thin strips between perforations continued to sustain the tensile force and exhibited good ductility. These strips can elongate from 6 mm up to 33 mm, which

may be considered beneficial in cases where the cell-wall sustains minor damage along its edge when buried beneath the ground.

4. The creep behavior of geocells was investigated on the cell-wall under 60%, 65% and 70% of its ultimate tensile strength (UTS). As expected, all specimens elongated considerably under a static load over the 300-hour applied loading period. The cell-wall maintained sound integrity when it is loaded by 60% UTS. By increasing the load by 5% UTS did not result in distinctly higher axial strain while slight deflections were found adjacent to the edge-perforations. At 70% UTS, although the cell-wall was only subjected an addition 5% increment, cell-wall exhibited pronounced and more rapid deformation; cell-wall ruptured at the edge-perforations and was close to failure.
5. A shrinkage ratio was developed to express the reduction in the height of the geocell wall with the application of the tensile, creep load. The shrinkage ratio is defined as the reduction in geocell height (mm) divided by the maximum elongation (mm) of each specimen (perpendicular to the height), at the cessation of the creep load application. It can be concluded that the shrinkage ratio is inversely proportional to the applied load. In other words, a greater load results in higher shrinkage, which indicates that geocell cell-wall is highly elastic under long-term loading. This may be considered to be a desirable feature in the practical application of geocells.
6. The geocell junctions did not exhibit significant improvement in the uniaxial tensile strength tests when compared to the geocell wall. Although a geocell

junction is the welded formation of two cell-wall strips, a modest average increase in tensile strength of 20% was recorded.

7. The results of the peeling and splitting strength tests show significant differences in peak strengths, but very similar trends in both the elastic and plastic regions. The ascending rate of the stress-elongation curves is slower when compared with those derived from the uniaxial tensile and shear loading cases.
8. When the junction is subjected to peeling and splitting, two types of failure modes were observed: cell-wall failures adjacent to the junctions; and weld failures where the cell-wall strips completely separated from one another. It should be noted that, when weld failure occurs, the specimen typically exhibits a lower peak strength.
9. When geocell junctions were subjected to shear, the specimens did not experience shear failure at the junctions, rather all failures occurred in the cell-wall. Therefore, it is suggested that the test results be considered as a lower bound of the shear strength of the geocell junctions.
10. A ductility ratio was proposed to quantify the rate of failure for each loading case, in both the cell-walls and junctions, under short-term loading. A higher ratio indicates that the failure occurs relatively rapidly, whereas a lower ratio indicates a more gradual failure. The geocell junction fails more suddenly under uniaxial tensile and shear loading than as a result of peeling or splitting.

5. REFERENCES

ASTM, 1993. Geosythetic Soil Reinforcement Testing Procedures. ASTM, Philadelphia, United State.

ASTM, 1996. Standard Test Method for Trapezoidal Tearing Strength of Geotextiles. ASTM D4533 - 91.

ASTM, 2004. Standard Test Method for Tensile Properties of Plastics, ASTM D638-03. ASTM International, PA, US.

ASTM, 2010. Standard Test Method for Density of Plastics by the Density-Gradient Technique, ASTM D1505 - 10. ASTM, PA, USA.

ASTM, 2016. D5262-07 Standard Test Method for Evaluating the Unconfined Tension Creep and Creep Rupture Behavior of Geosynthetics. American Society for Testing and Materials, Pennsylvania, USA.

Becker, L.D.B., Nunes, A.L.L.d.S., 2015. Influence of soil confinement on the creep behavior of geotextiles. Geotextiles and Geomembranes 43, 351-358.

Choi, B.-H., Weinhold, J., Reuschle, D., Kapur, M., 2009. Modeling of the fracture mechanism of HDPE subjected to environmental stress crack resistance test. Polymer Engineering & Science 49, 2085-2091.

Dash, S.K., Shivadas, A.S., 2012. Performance Improvement of Railway Ballast Using Geocells. Indian Geotechnical Journal 42, 186-193.

Hegde, A., Sitharam, T.G., 2015a. 3-Dimensional numerical modelling of geocell reinforced sand beds. Geotextiles and Geomembranes 43, 171-181.

Hegde, A.M., Sitharam, T.G., 2015b. Three-dimensional numerical analysis of geocell-reinforced soft clay beds by considering the actual geometry of geocell pockets. Canadian Geotechnical Journal 52, 1396-1407.

Kwon, H.J., Jar, P.Y.B., 2008. On the application of FEM to deformation of high-density polyethylene. International Journal of Solids and Structures 45, 3521-3543.

Leshchinsky, B., Ling, H., 2013. Effects of Geocell Confinement on Strength and Deformation Behavior of Gravel. Journal of Geotechnical and Geoenvironmental Engineering 139, 340-352.

Liu, Y., Deng, A., Jaksa, M., 2018. Three-dimensional modeling of geocell-reinforced straight and curved ballast embankments. Computers and Geotechnics 102, 53-65.

Meuller, W.W., 2007. HDPE Geomembranes in Geotechnics. Springer Berlin Heidelberg, Berlin.

Ngo, N.T., Indraratna, B., Rujikiatkamjorn, C., Mahdi Biabani, M., 2015. Experimental and Discrete Element Modeling of Geocell-Stabilized Subballast Subjected to Cyclic Loading. Journal of Geotechnical and Geoenvironmental Engineering, 04015100.

Pan, H., Devasahayam, S., Bandyopadhyay, S., 2017. Study of microstructure and fracture properties of blunt notched and sharp cracked high density polyethylene specimens. Sci Rep 7, 6096.

Pokharel, S.K., Han, J., Leshchinsky, D., Parsons, R.L., Halahmi, I., 2010. Investigation of factors influencing behavior of single geocell-reinforced bases under static loading. Geotextiles and Geomembranes 28, 570-578.

Sawicki, A.K.-F., K., 1998. Creep behaviour of geosynthetics. Geotextiles and Geomembranes 16, 365-382.

Shadmand, A., Ghazavi, M., Ganjian, N., 2018. Load-settlement characteristics of large-scale square footing on sand reinforced with opening geocell reinforcement. Geotextiles and Geomembranes 46, 319-326.

Song, F., Liu, H., Chai, H., Chen, J., 2017. Stability analysis of geocell-reinforced retaining walls. Geosynthetics International 24, 442-450.

Suku, L., Prabhu, S.S., Ramesh, P., Babu, G.L.S., 2016. Behavior of geocell-reinforced granular base under repeated loading. Transportation Geotechnics 9, 17-30.

Tanyu, B.F., Lau, A.W., Edil, T.B., Benson, C.H., Aydilek, A.H., 2013. Laboratory evaluation of geocell-reinforced gravel subbase over poor subgrades. Geosynthetics International 20, 47-61.

Tariq, F., Naz, N., Khan, M.A., Baloch, R.A., 2011. Failure analysis of high density polyethylene butt weld joint. Journal of Failure Analysis and Prevention 12, 168-180.

Thakur, J.K., Han, J., Parsons, R.L., 2013. Creep behavior of geocell-reinforced recycled asphalt pavement bases. Journal of Material in Engineering 25, 1533-1542.

Venkateswarlu, H., Ujjawal, K.N., Hegde, A., 2018. Laboratory and numerical investigation of machine foundations reinforced with geogrids and geocells. Geotextiles and Geomembranes 46, 882-896.

Wu, K.J., Austin, D.N., 1992. Three-dimensional polyethylene geocells for erosion control and channel linings. Geotextiles and Geomembranes 11, 611-620.

Yang, X., Han, J., Pokharel, S.K., Manandhar, C., Parsons, R.L., Leshchinsky, D., Halahmi, I., 2012. Accelerated pavement testing of unpaved roads with geocell-reinforced sand bases. Geotext Geomembr 32, 95-103.

Zhang, L., Zhao, M., Shi, C., Zhao, H., 2010. Bearing capacity of geocell reinforcement in embankment engineering. Geotextiles and Geomembranes 28, 475-482.

LIST OF TABLE

Table 1. Specimen dimensions.

Test	Junction thickness (mm)	Junction length (mm)	Overall length (mm)	Clamping distance (mm)
Tensile & Shear strength	3.5	10.5	120.5	10.5
Seam & Split strength	3.5	10.5	110	30

Table 2. Specimen designation.

Specimen type	Test	Designation
Geocell wall	Uniaxial tensile strength	CW-UTS
	Trapezoidal tearing strength	CW-TTS
	Creep	CW-CT
Geocell junction	Uniaxial tensile strength	J-UTS
	Shear strength	J-SS
	Seam strength	J-SMS
	Split strength	J-SPS

Table 3. Shrinkage ratios of three tested specimens.

	Specimen 1 (0.49 kN loading)	Specimen 2 (0.54 kN loading)	Specimen 3 (0.58 kN loading)
Maximum elongation (mm)	24.81	27.35	65.24
Shrinkage (mm)	19.67	16.83	34.6
Shrinkage ratio (%)	79.28	61.54	53.04

Table 4. Ductility ratio for geocell walls and junctions under different test conditions.

Test	Specimen	Elongation (mm)		Ductility	Average
		Pre-peak	Post-peak		
Uniaxial tensile strength (cell-wall)	1	10.05	44.22	4.40	5.45
	2	13.16	33.09	2.52	
	3	11.98	110.61	9.23	
	4	12.89	33.16	2.57	
	5	12.37	105.29	8.52	
Trapezoidal tearing strength (cell-wall)	1	43.61	113.60	2.60	2.63
	2	49.89	172.98	3.47	
	3	51.16	140.65	2.75	
	4	47.20	90.87	1.93	
	5	47.65	109.68	2.30	
Uniaxial tensile strength (Junction)	1	3.77	20.52	5.44	12.17
	2	3.63	46.99	12.94	
	3	3.37	55.28	16.42	
	4	4.36	47.54	10.89	
	5	3.57	53.98	15.14	
Shear strength (Junction)	1	1.56	27.83	17.84	11.02
	2	2.11	26.36	12.49	
	3	2.39	15.88	6.65	
	4	2.55	16.70	6.56	
	5	2.51	28.91	11.53	
Split strength (Junction)	1	14.15	14.06	0.99	0.95
	2	12.62	12.98	1.03	
	3	12.90	15.34	1.19	
	4	15.99	11.95	0.75	
	5	10.19	8.29	0.81	
Seam strength (Junction)	1	15.75	12.70	0.81	0.74
	2	21.47	16.15	0.75	
	3	18.59	7.71	0.41	
	4	20.87	12.10	0.58	
	5	20.47	23.78	1.16	

LIST OF FIGURES

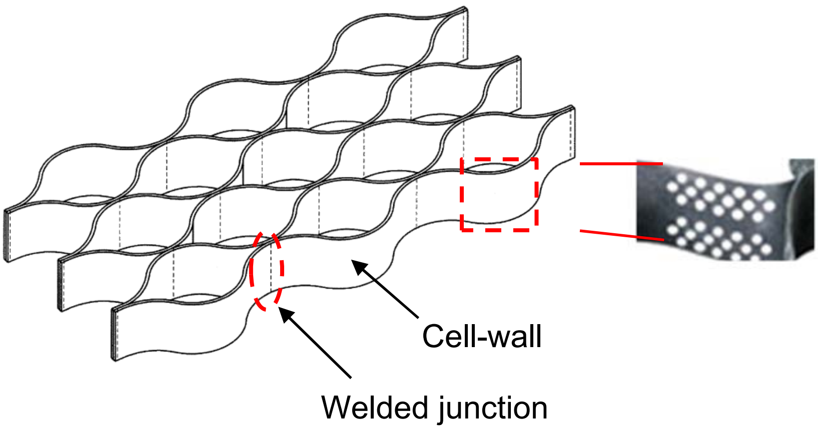

Figure 1. Geocell components.

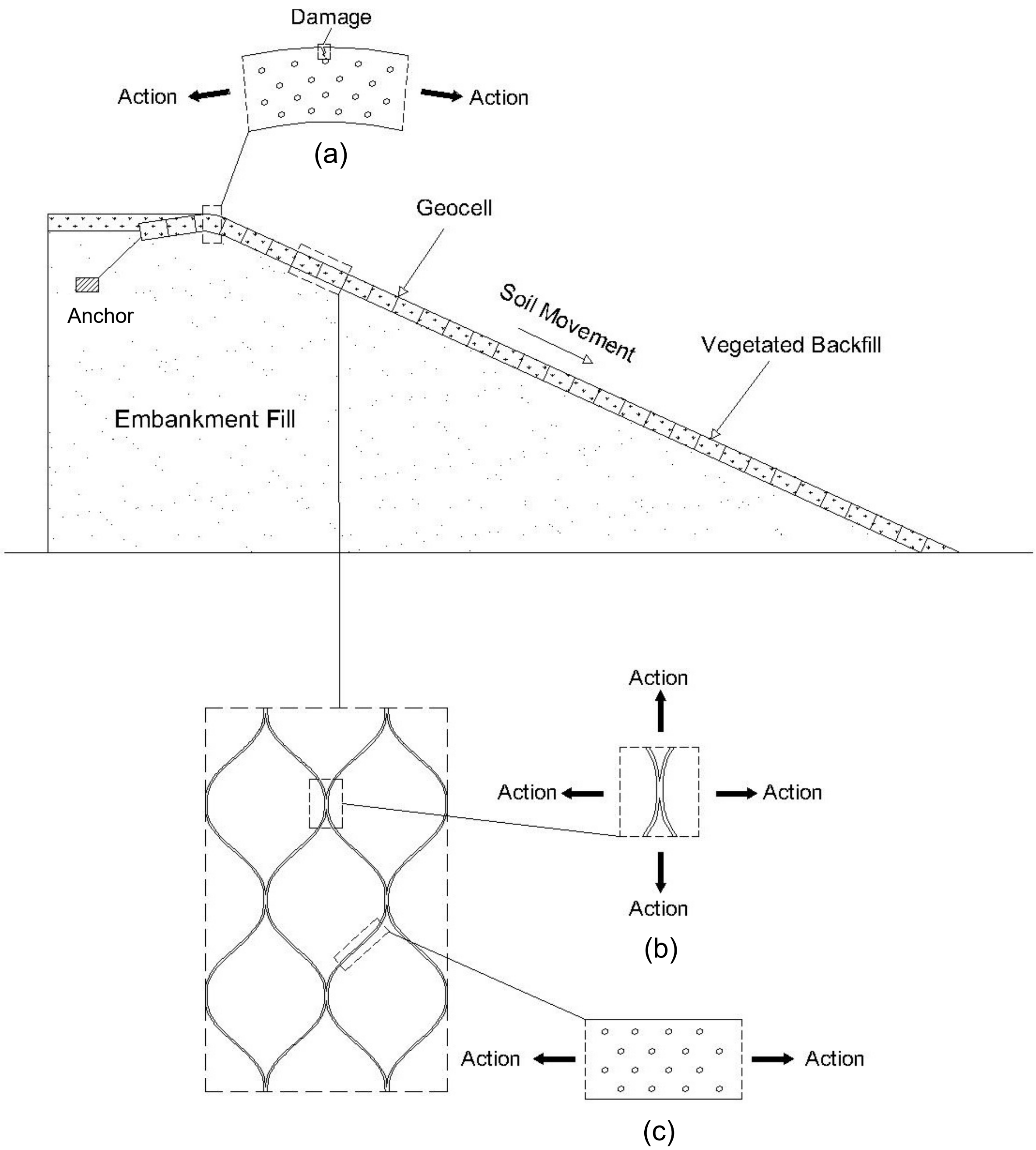

Figure 2. Typical geocell application in slope stabilization and the force induced by soil movement at different locations.

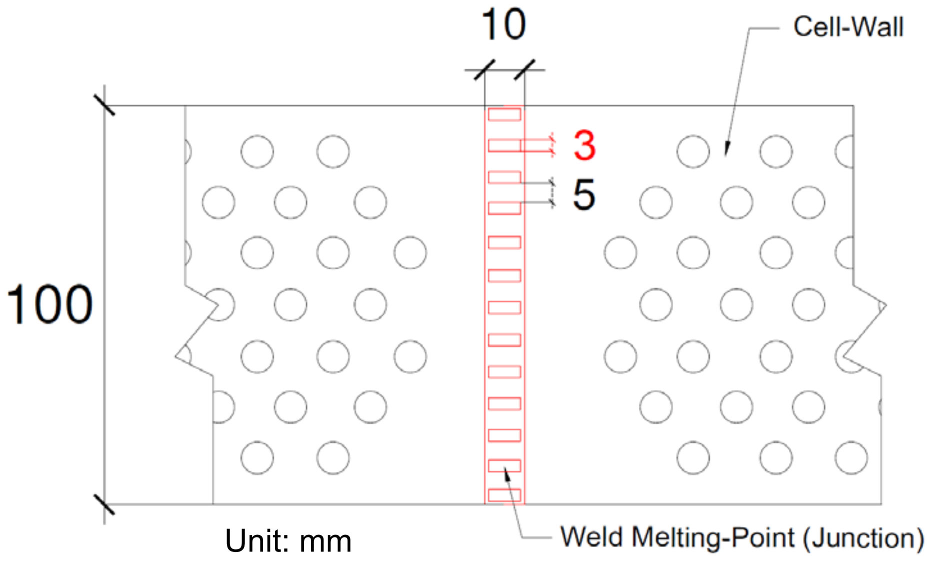

Figure 3. Details of the geocell junction

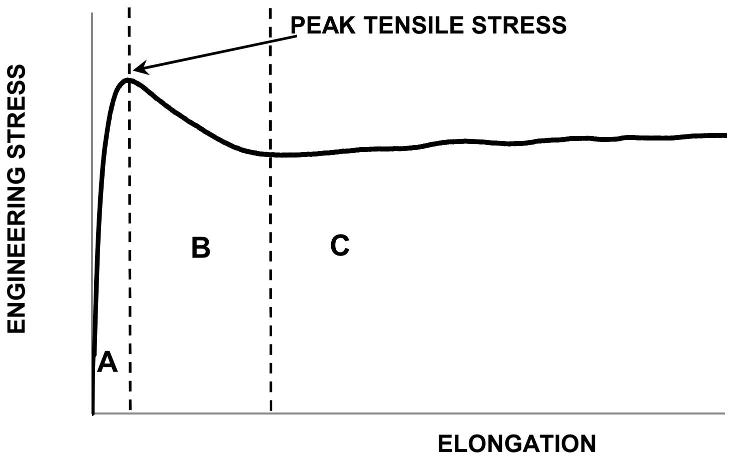

Figure 4. Typical stress-displacement relationship of HDPE (Kwon and Jar, 2008).

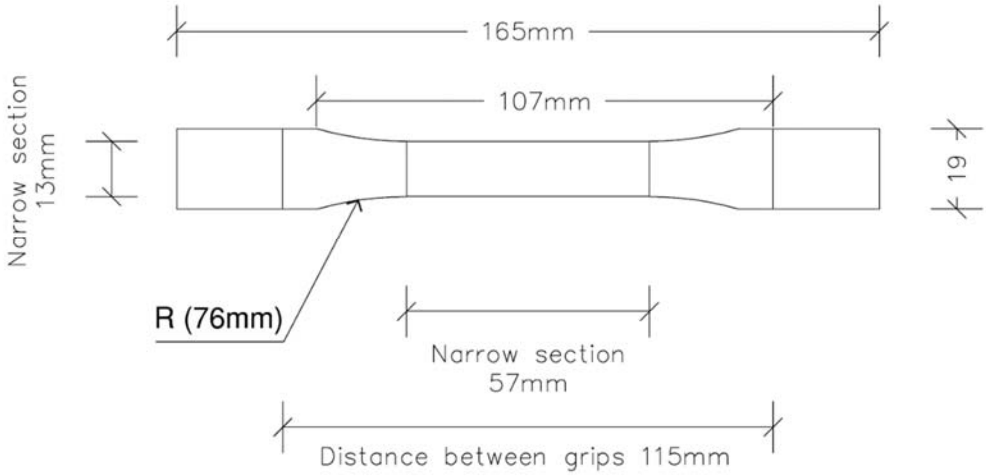

(a)

(b)

Figure 5. Uniaxial tensile strength test on geocell wall: (a) specimen configurations, (b) testing overview.

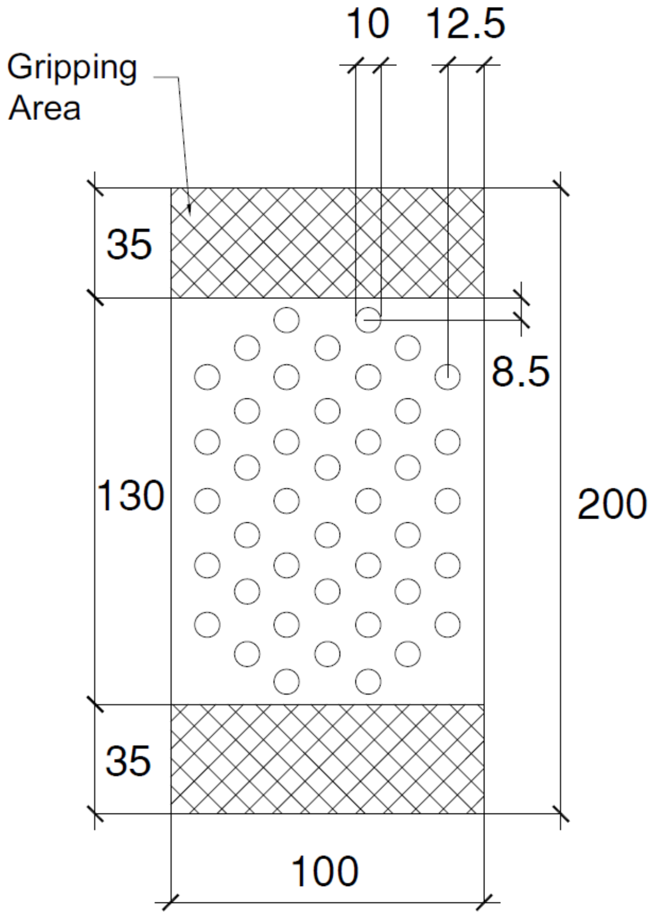

Figure 6. Prepared sample and dimension.

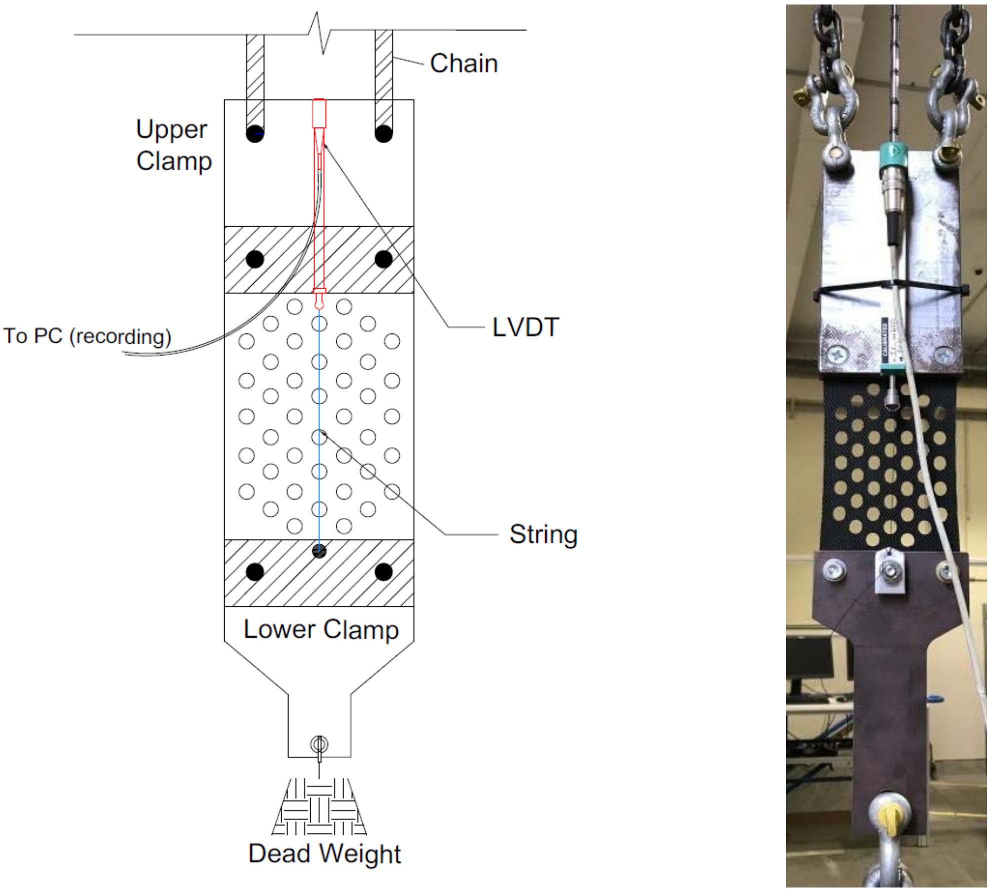

(a) (b)

Figure 7. Creep test: (a) schematic and (b) test setup.

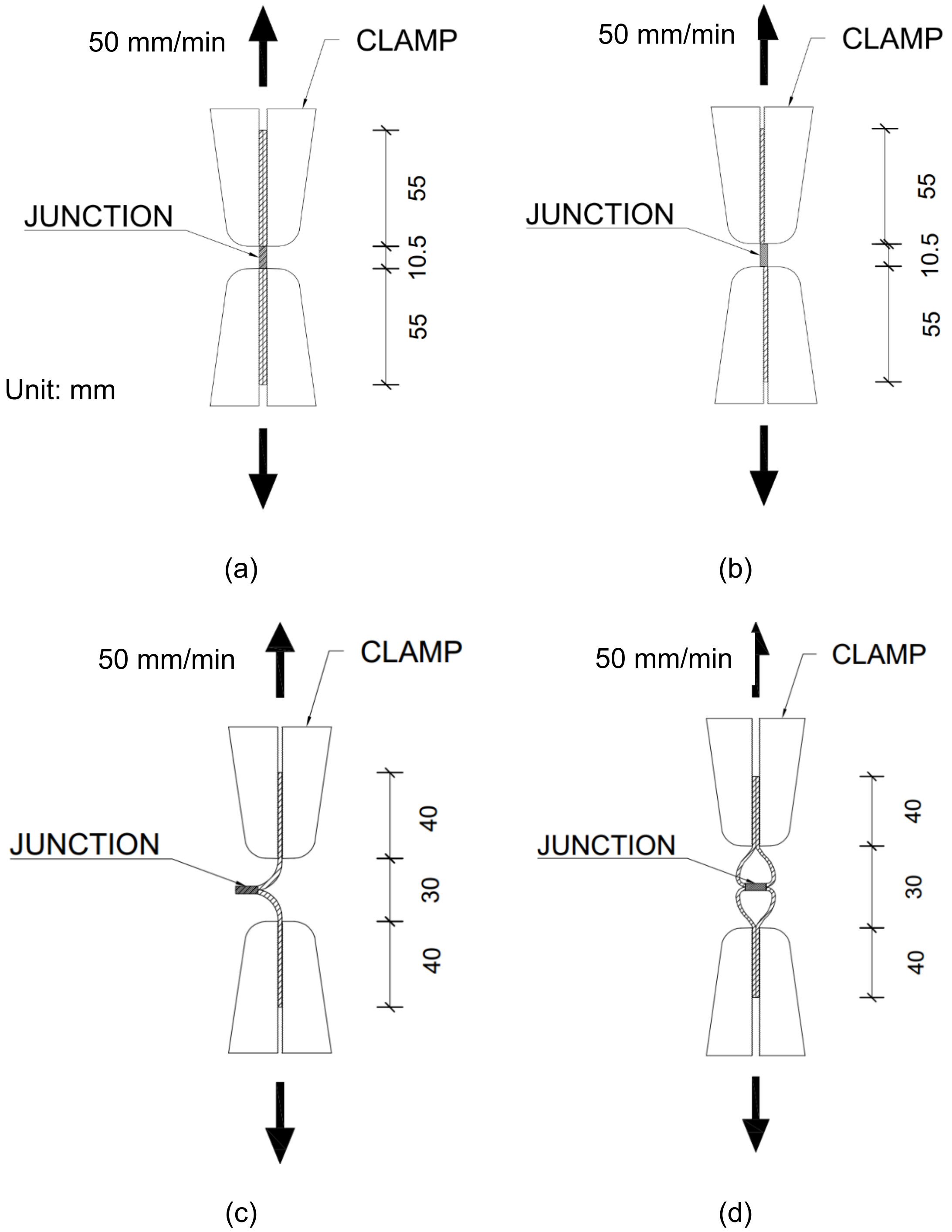

Figure 8. Junction strength tests: (a) uniaxial tensile strength, (b) shear strength, (c) peel strength and (d) split strength.

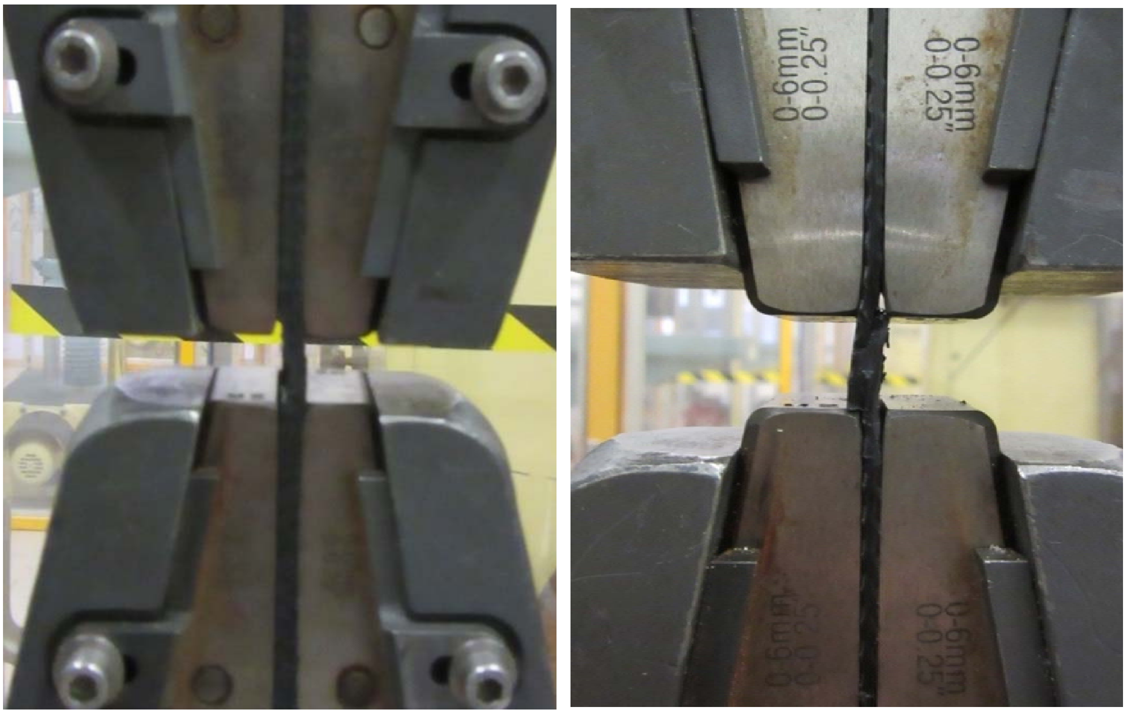

(a) (b)

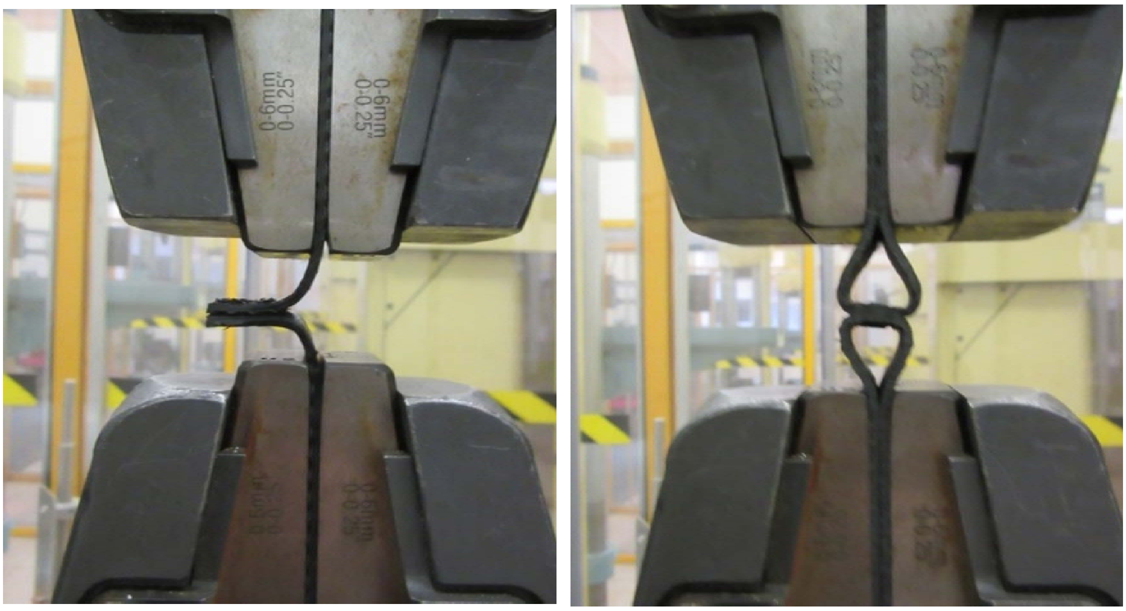

(c) **(d)**

Figure 9. Clamped specimens: (a) tensile strength, (b) shear junction strength, (c) seam strength, and (d) split strength.

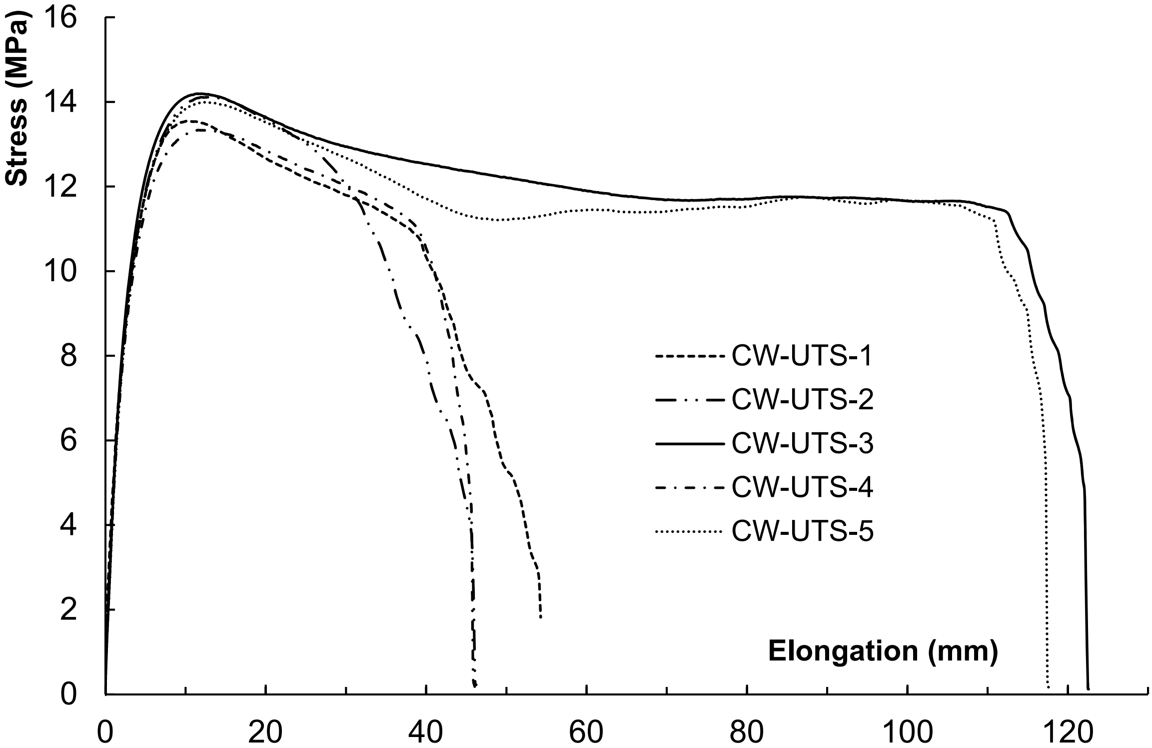

Figure 10. Stress–elongation relationship of geocell cell-wall subjected to uniaxial tensile force.

(a)

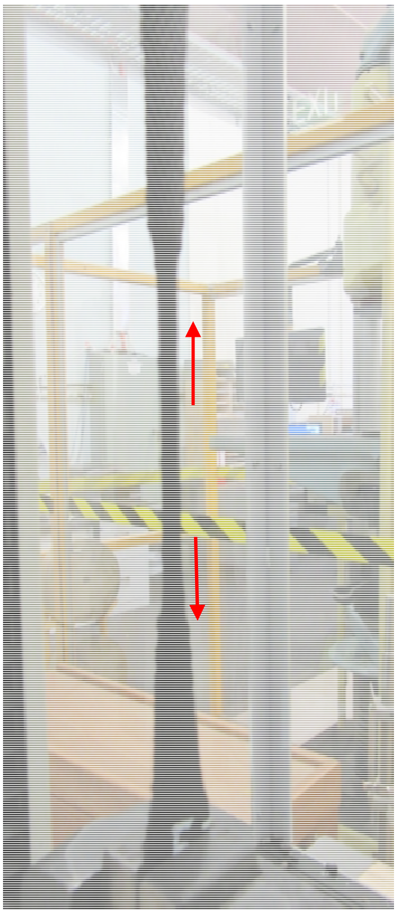

(b)

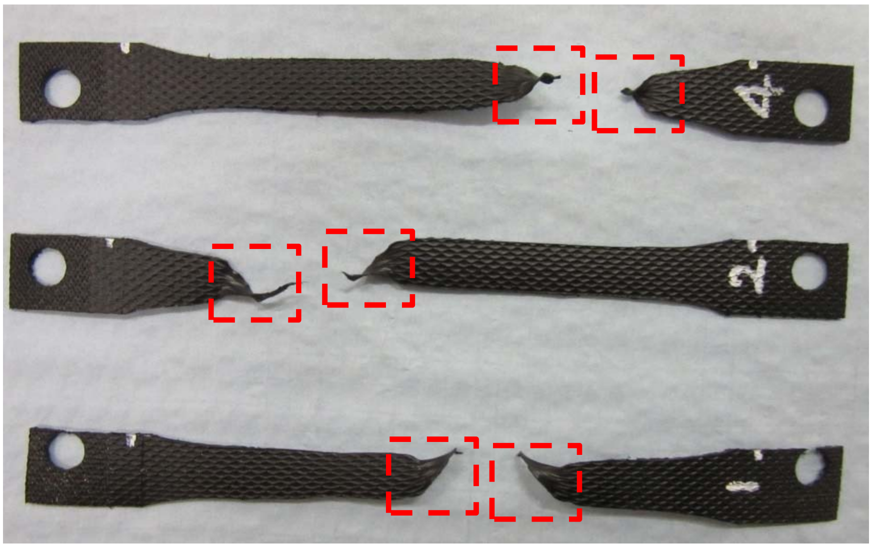

(c)

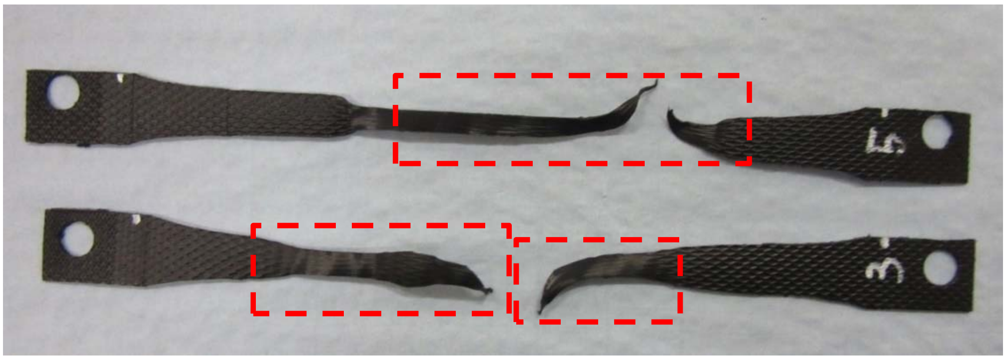

(d)

Figure 11. Failure modes of cell-wall specimens subjected to uniaxial tension: (a) and (c) sudden failure, (b) and (d) ductile failure mode of HDPE.

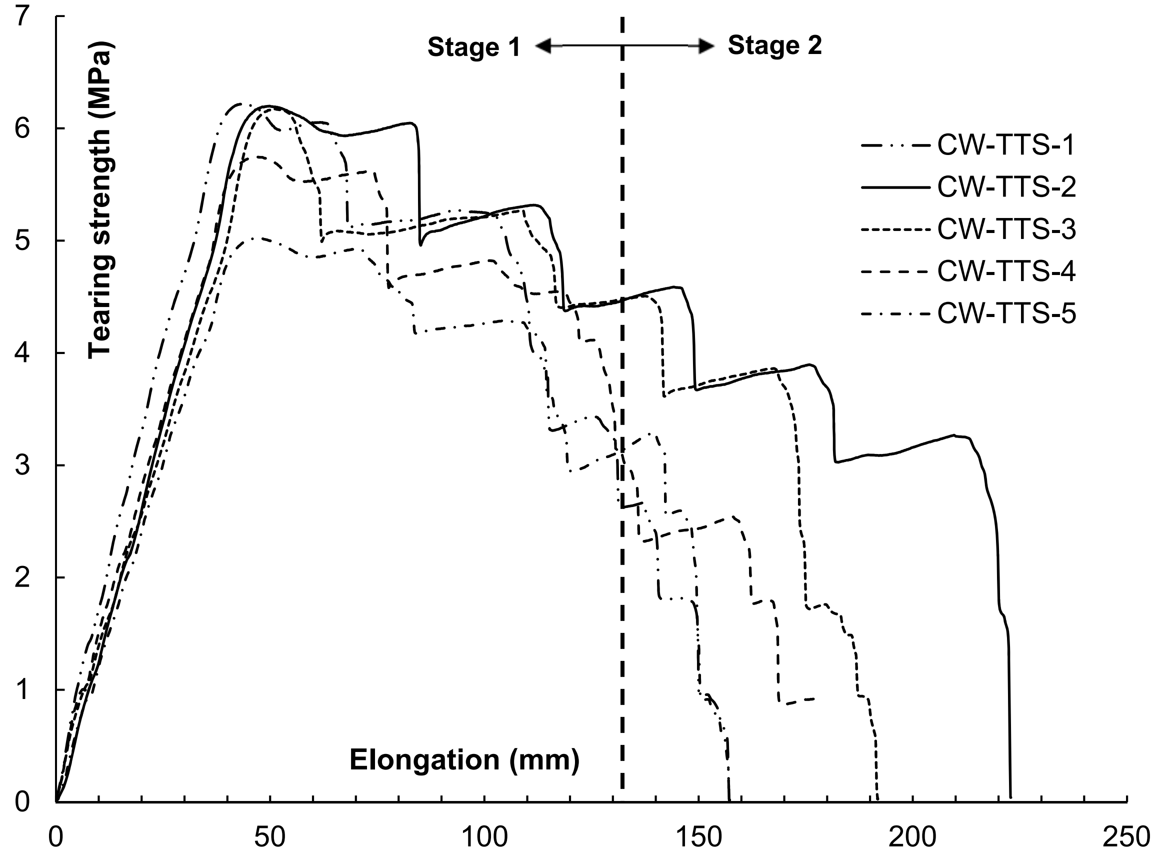

Figure 12. Force-elongation relationship of geocell cell-wall subject to tearing.

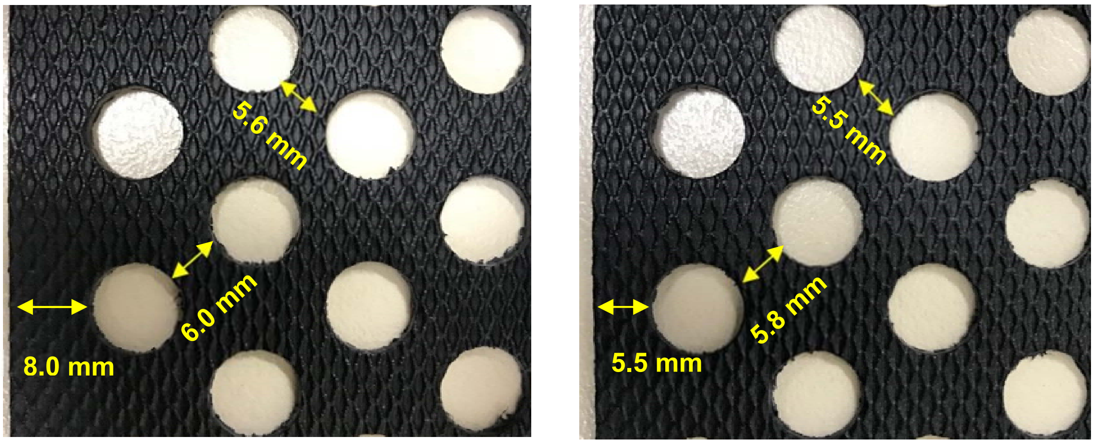

(a) (b)

Figure 13. Inconsistencies in perforations between two cell-wall specimens: (a) specimen A, (b) specimen B.

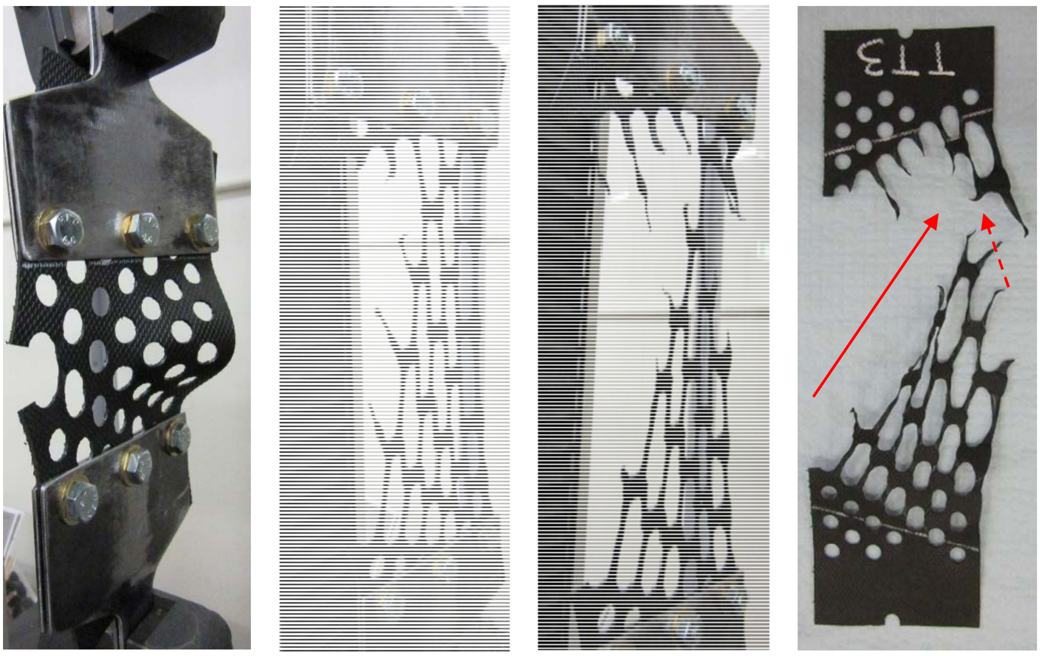

(a) (b) (c) (d)

Figure 14. The progressive failure of cell-wall specimen CW-TTS-3 at different elongations: (a) 0 mm, (b) 115 mm, (c) 180 mm and (d) failure pattern.

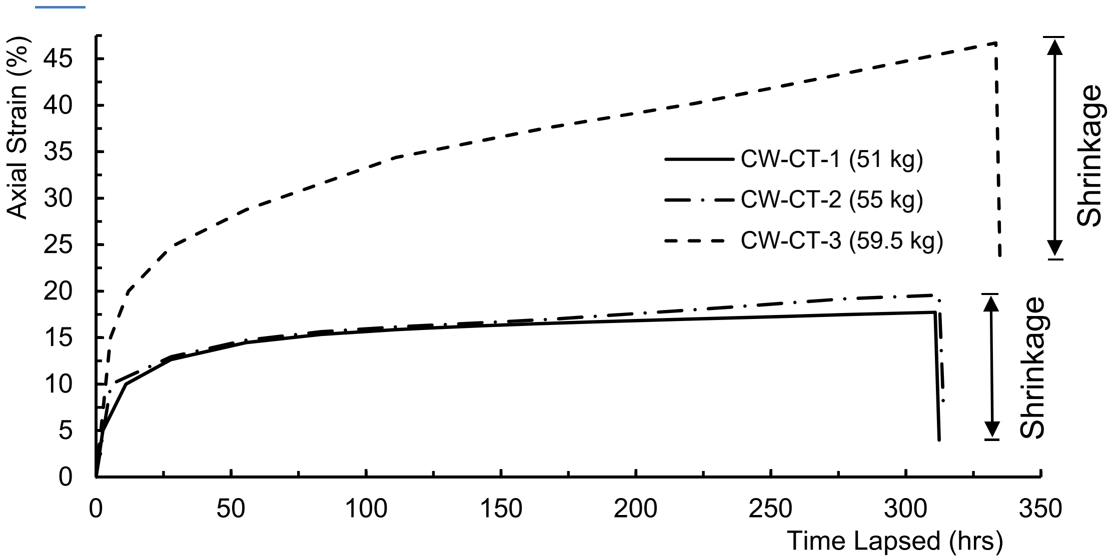

(a)

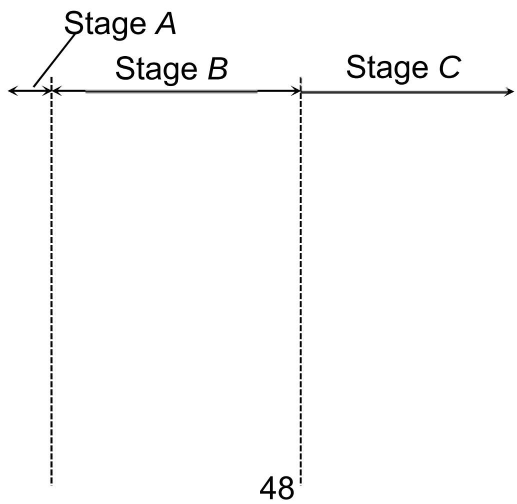

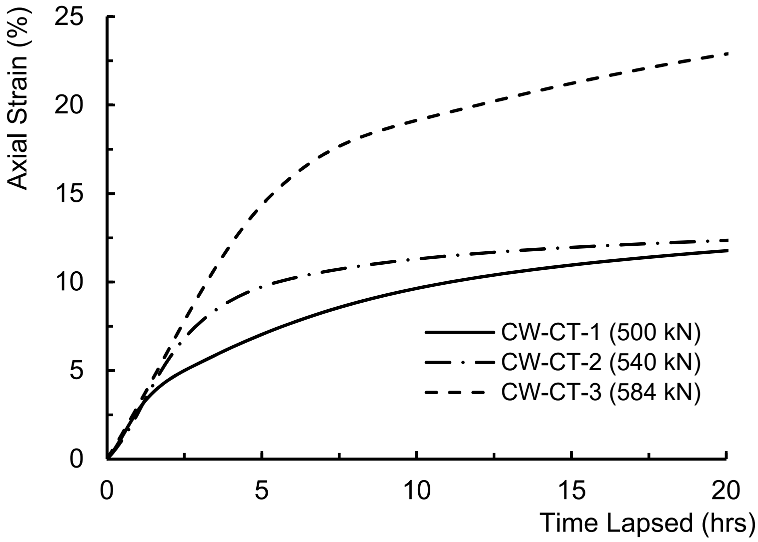

(b)

Figure 15. Strain-time relationship of three tested specimens.

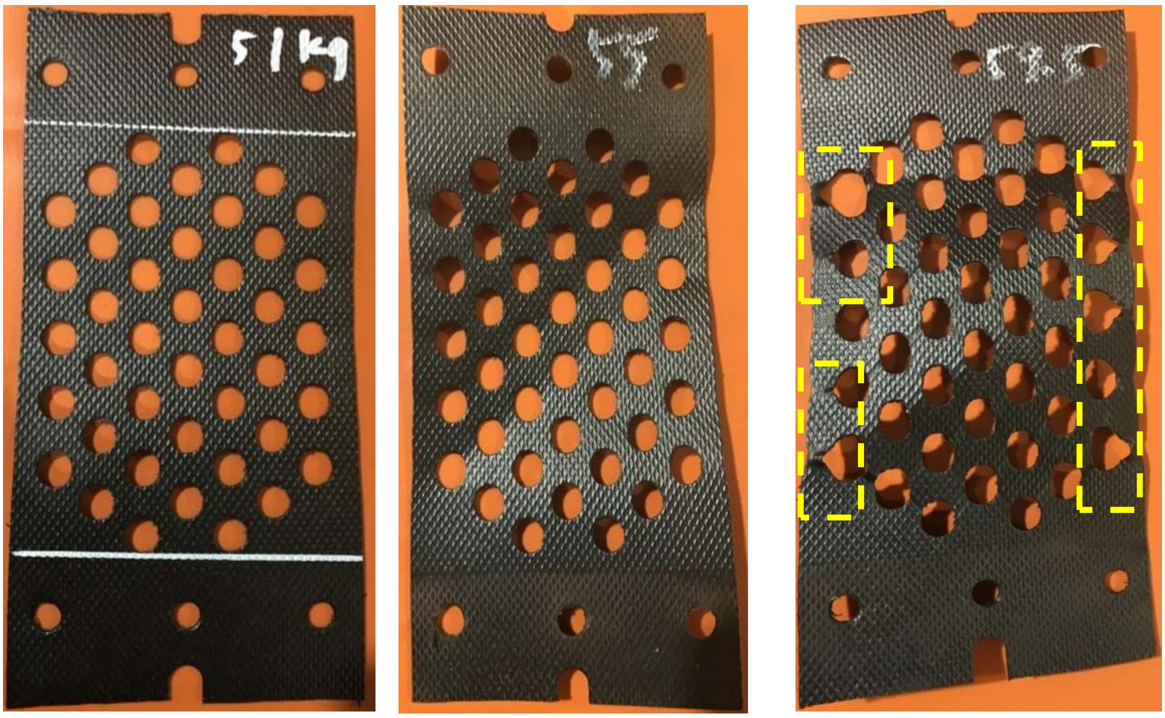

(a) (b) (c)

Figure 16. Final form of specimens: (a) specimen 1 (0.49 kN loading), (b) specimen 2 (0.54 kN loading), (c) specimen 3 (0.58 kN loading).

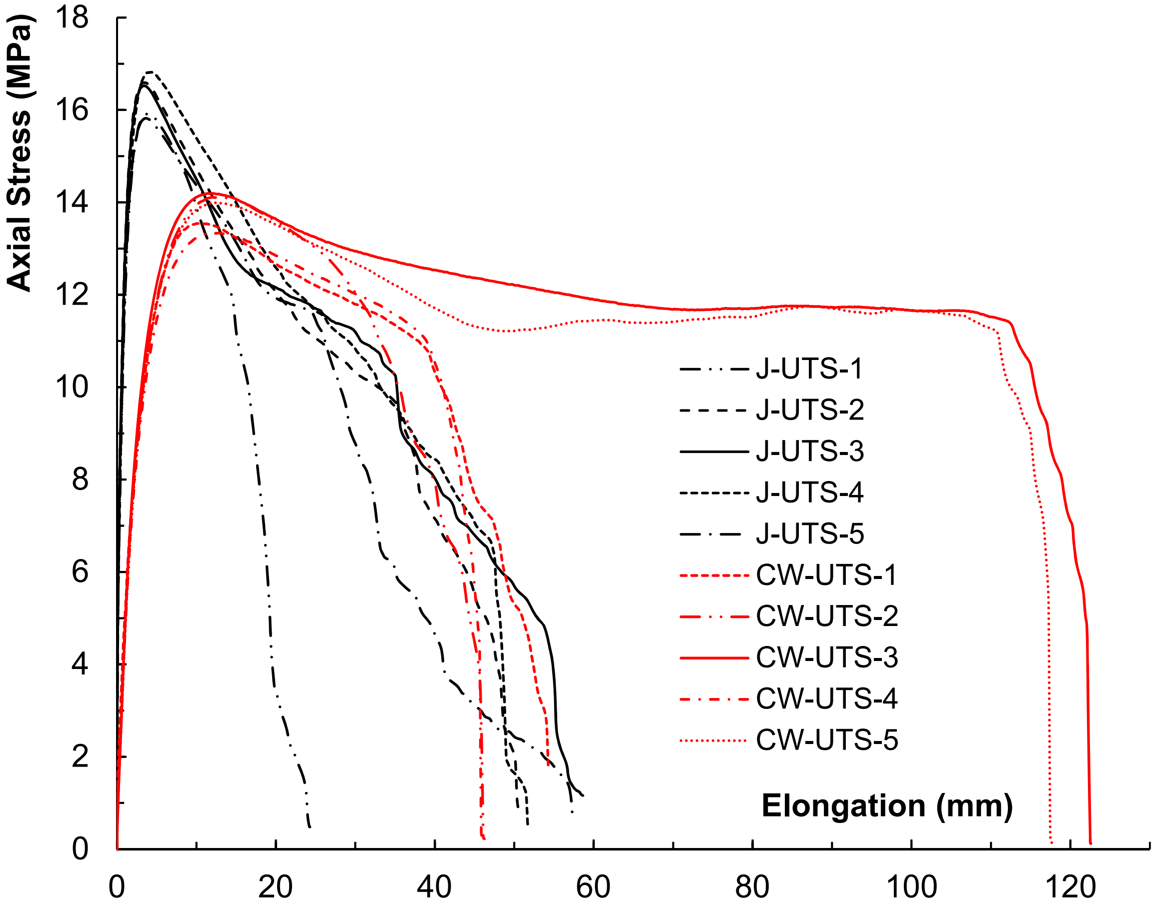

Figure 17. Stress-elongation relationship of the geocell junction subjected to a uniaxial tensile force.

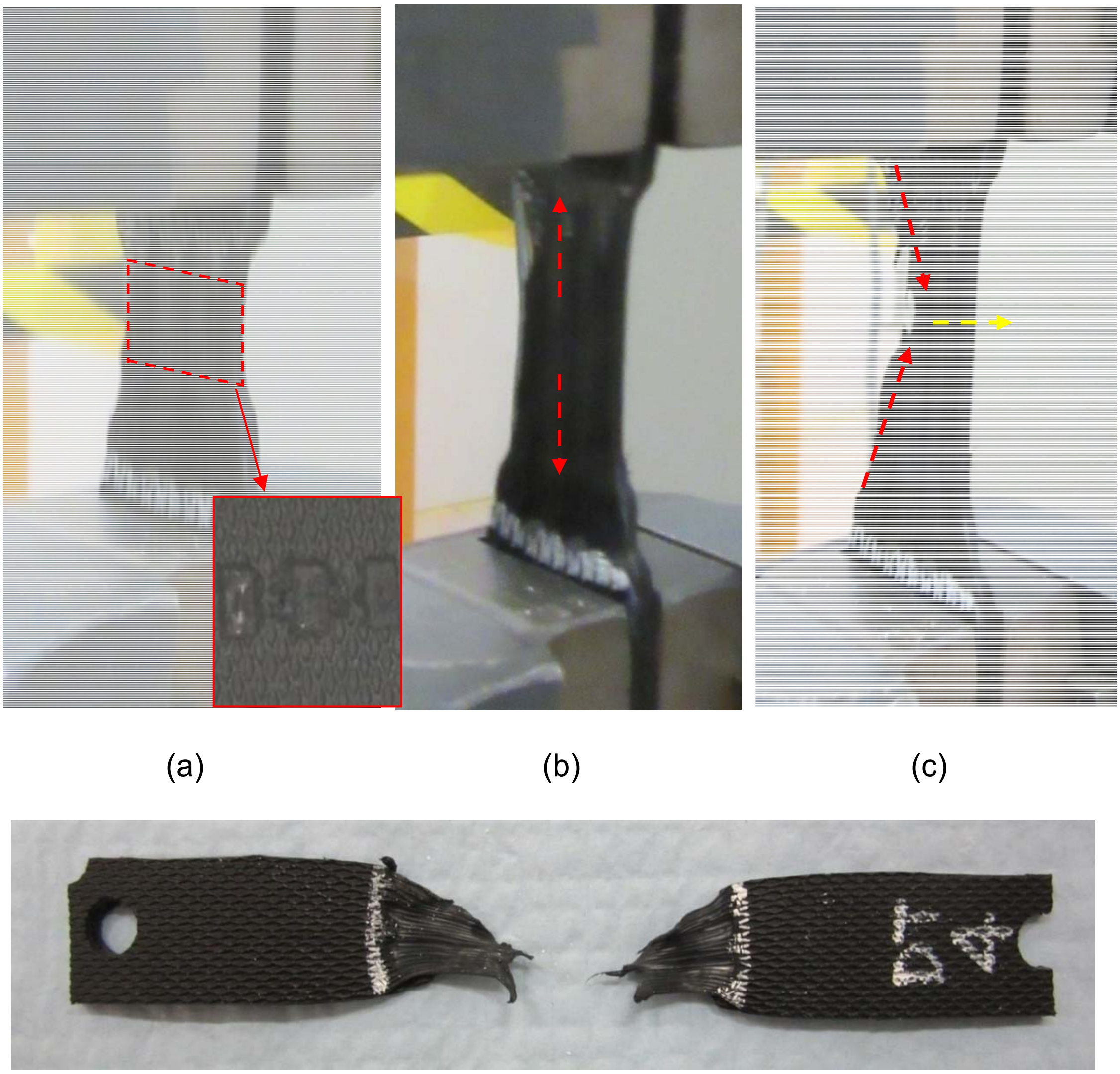

(a) (b) (c)

(d)

Figure 18. Failure modes of the geocell junction subjected to uniaxial tension: (a) initial stage (pre-peak), (b) failure mode 1 (post-peak), (c) failure mode 2 (post-peak), and (d) ruptured specimen 1.

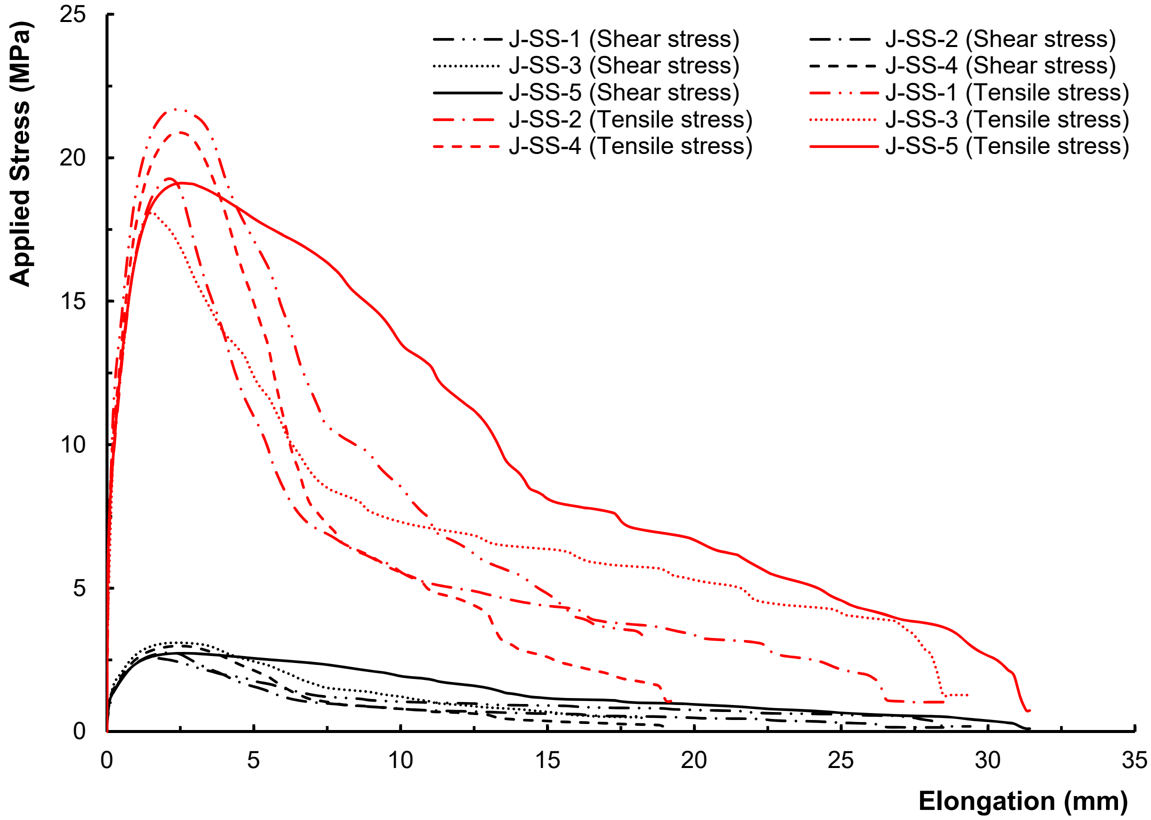

Figure 19. Force-elongation relationship of geocell junction subjected to shear force.

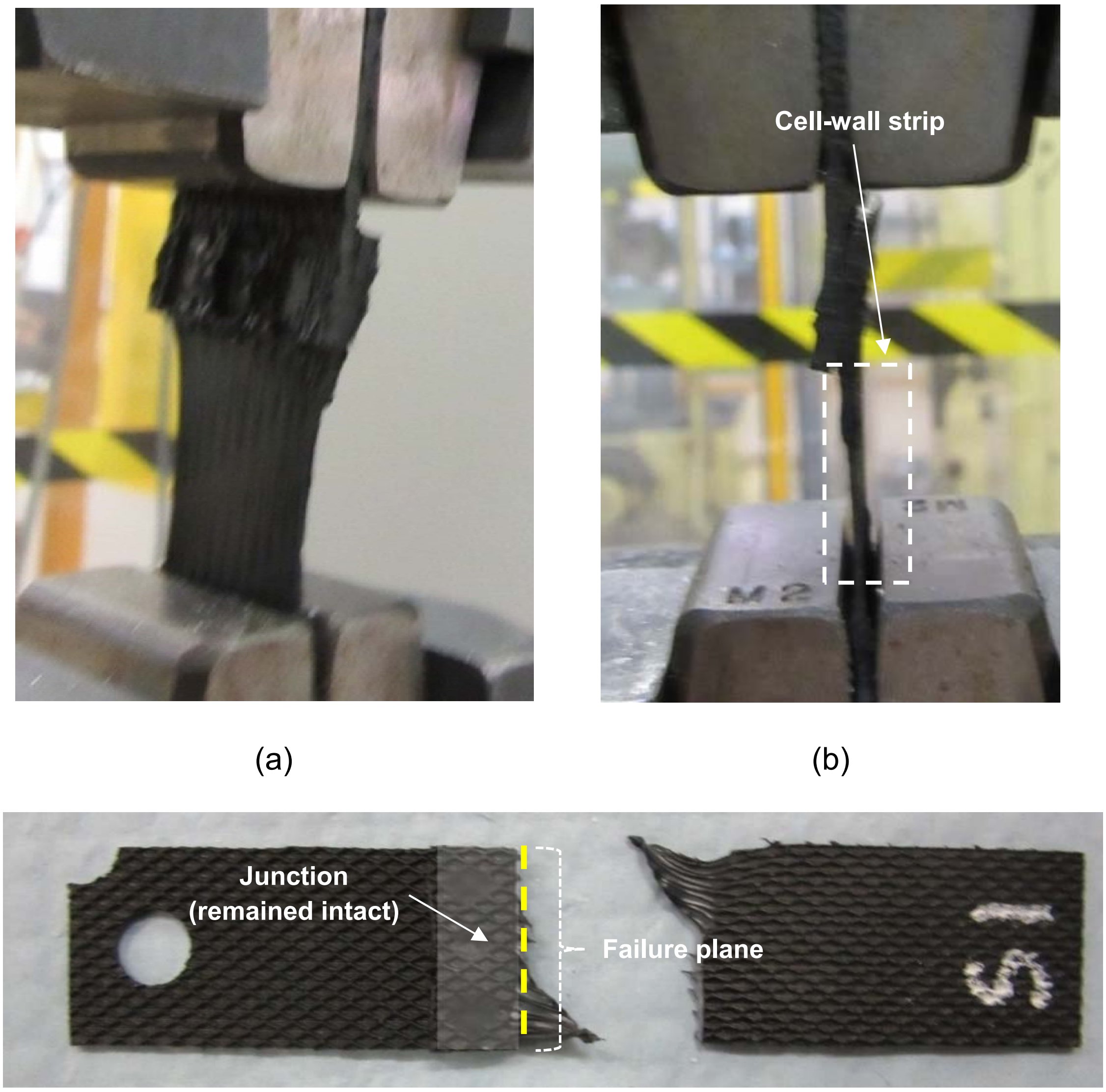

(c)

Figure 20. Failure modes of geocell junctions subjected to shear force: (a) oblique view and (b) side view during testing, and (c) failed specimen.

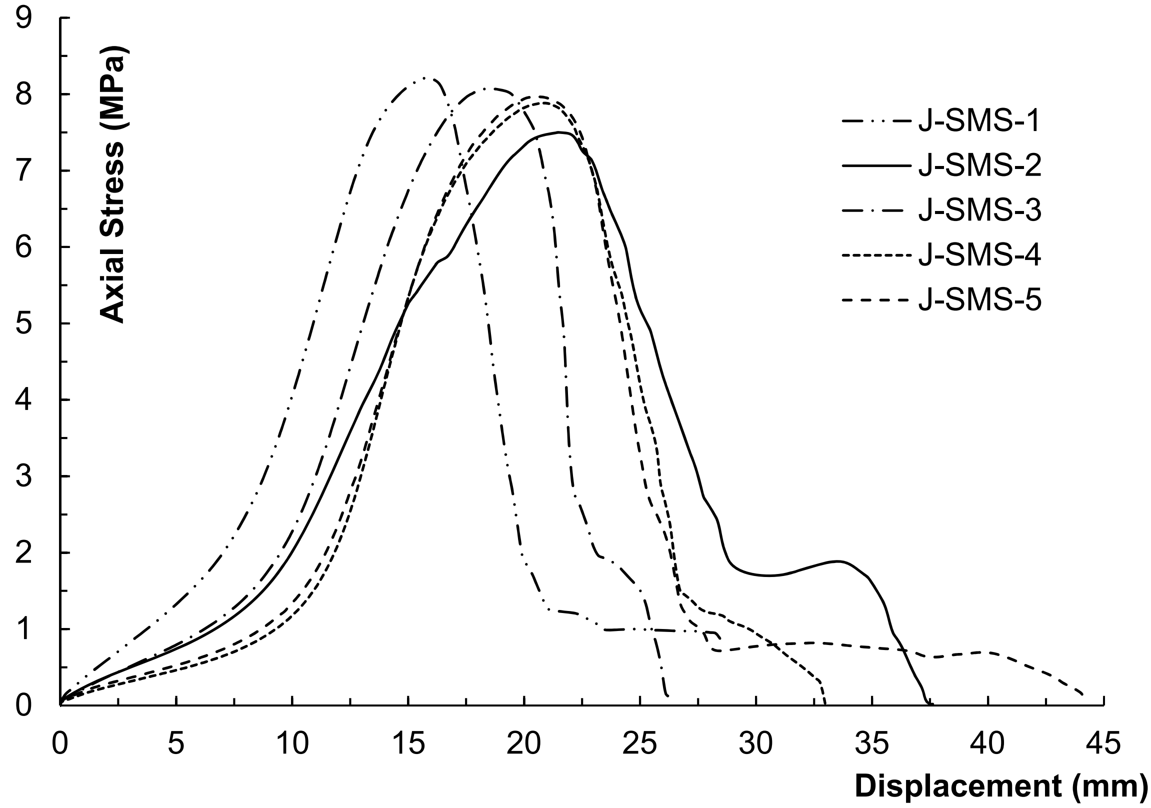

Figure 21. Stress-elongation relationship of tested geocell junctions when subjected to a peeling force.

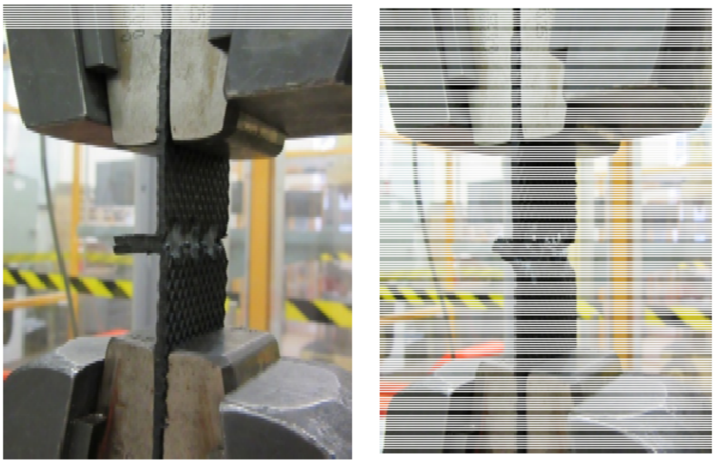

(a)

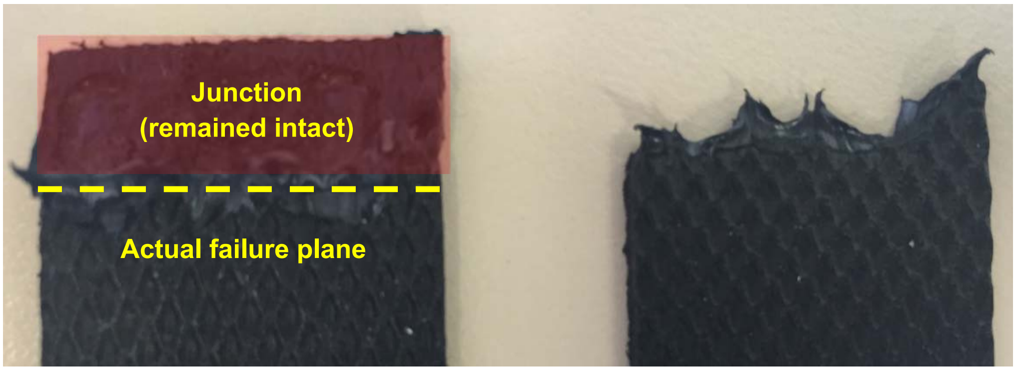

(b)

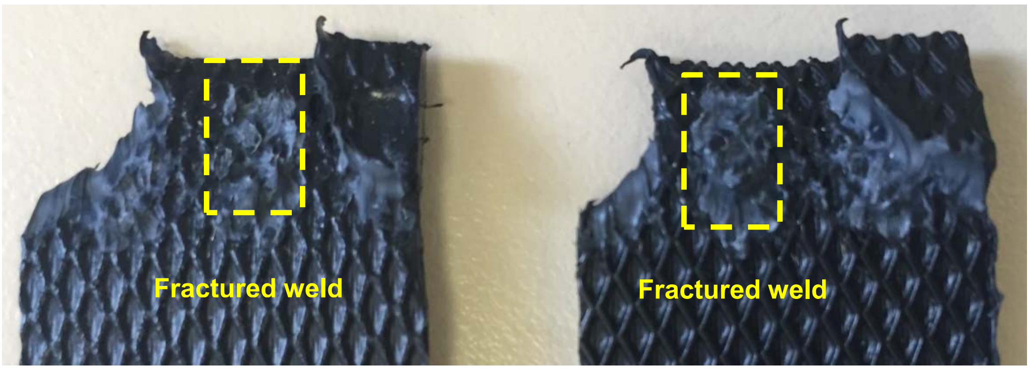

(c)

Figure 22. Failure modes of geocell junctions subjected to peeling force: (a) during testing, (b) strip failure, (c) weld failure.

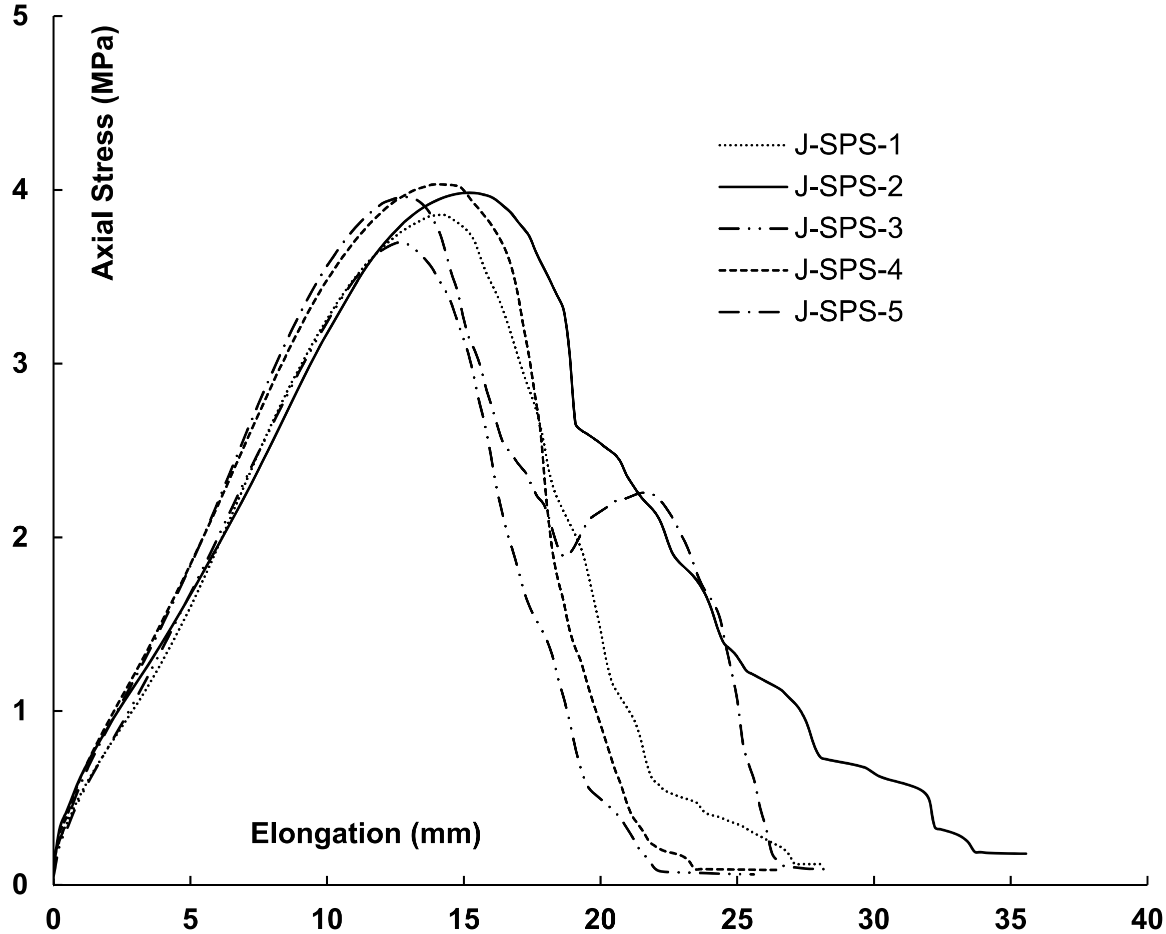

Figure 23. Stress-elongation relationship of geocell junctions subjected to splitting.

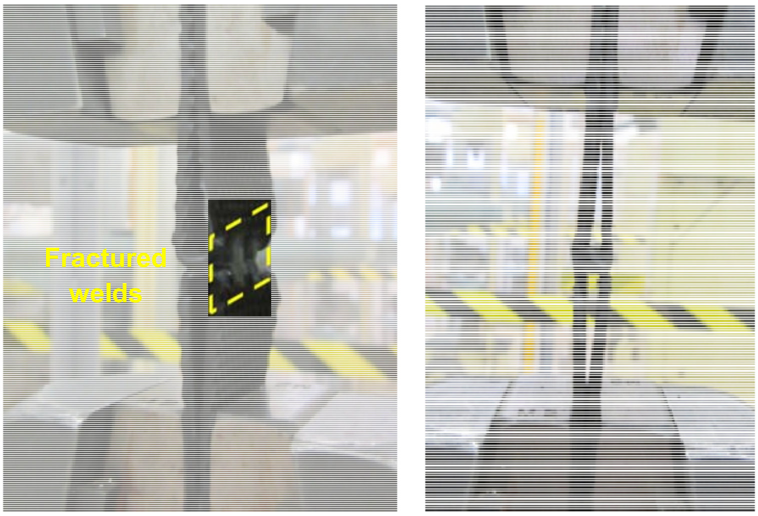

(a)

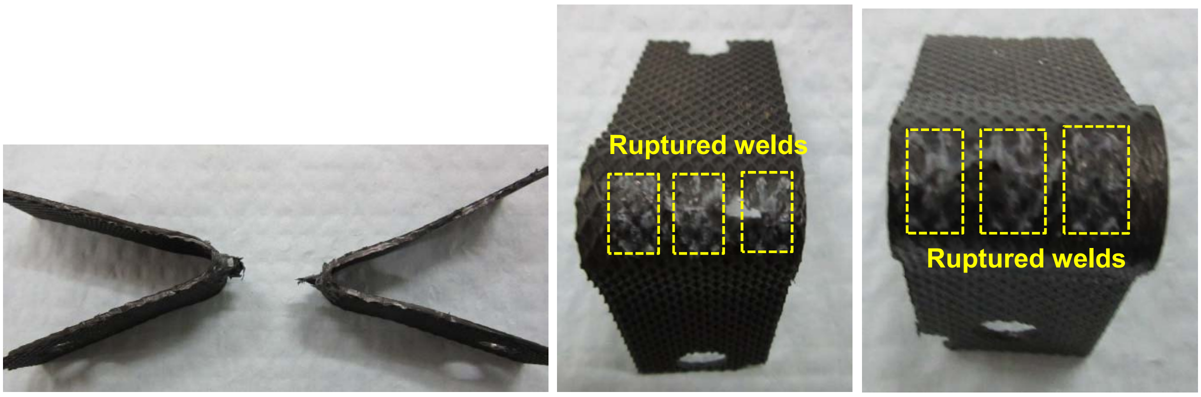

(b)

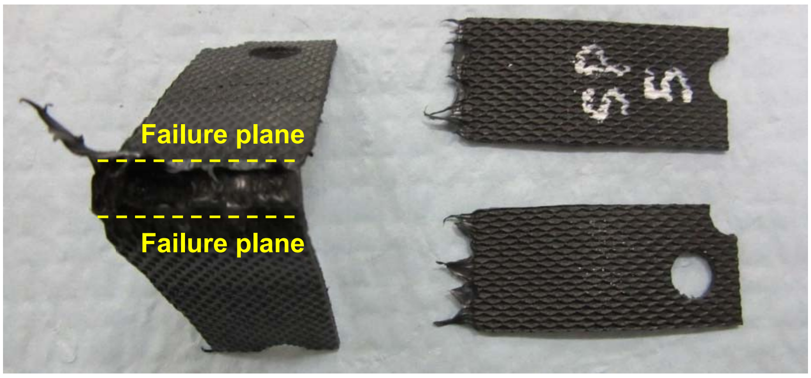

(c)

Figure 24. Failure modes of geocell junctions subjected to a splitting force: (a) during testing; (b) junction failure; (c) cell-wall strip failure.

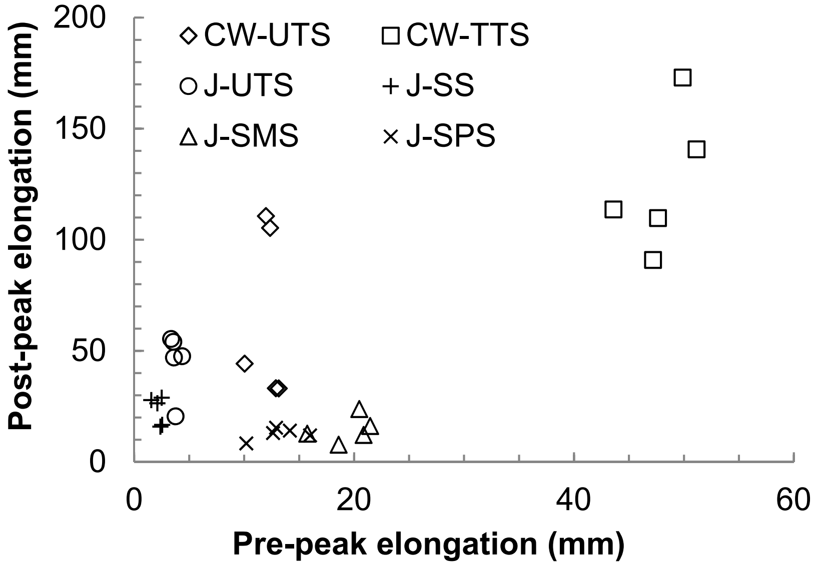

(a)

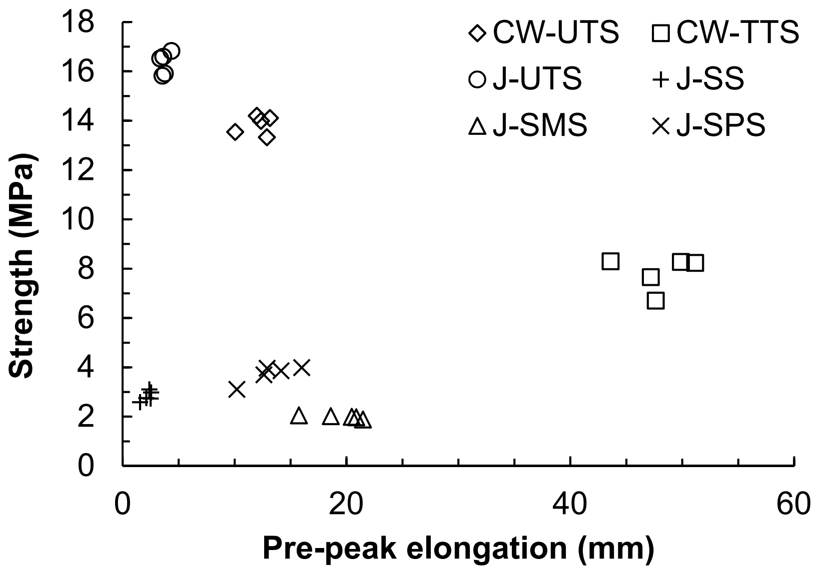

(b)

Figure 25. Cell-wall and junction test results: (a) post-peak elongation versus pre-peak elongation, (b) strength versus pre-peak elongation.